Study of the seakeeping non-linearities through the weak-scatterer approximation of the potential flow theory

Auteur : Sudhanshu,
Promoteur(s) : 14928
Faculté : Faculté des Sciences appliquées
Diplôme : Master : ingénieur civil mécanicien, à finalité spécialisée en "Advanced Ship Design"
Année académique : 2020-2021
URI/URL : http://hdl.handle.net/2268.2/13169

Study of the seakeeping non-linearities through the weak-scatterer approximation of the potential flow theory

Submitted on 26th August 2021 by **. Sudhanshu** | D223, 1 rue de la Noë | ECN, Nantes-44321 (France) | sudhanshulvs30@gmail.com | Student ID No.: S200244A

Contents

List of Figures

List of Tables

Declaration of Authorship

I declare that this thesis and the work presented in it are my own and have been generated by me as the result of my own original research.

Where I have consulted the published work of others, this is always clearly attributed.

Where I have quoted from the work of others, the source is always given. With the exception of such quotations, this thesis is entirely my own work.

I have acknowledged all main sources of help.

Where the thesis is based on work done by myself jointly with others, I have made clear exactly what was done by others and what I have contributed myself. This thesis contains no material that has been submitted previously, in whole or in part, for the award of any other academic degree or diploma.

I cede copyright of the thesis in favour of the Ecole Centrale de Nantes.

Date: 26th August 2021

Signature:

Acknowledgements

First and foremost, I would like to thanks with sincere gratitude to my supervisor, Moran Charlou for guiding and helping during last 5 months. He was always there for any small help specially during last few months post opening of the 2nd Covid lock-down. I would be also huge indebted to him for reviewing my work numerous times so that any mistake should be avoided.

Then, I would to thanks Professor Ph. Rigo, Lionel Gentaz and his EMship team for choosing me being part of the EMship and guiding me for this entire EMShip journey.

I would like thanks to LHEEA for providing opportunity to perform my master thesis, specially to LHEEA's IT team and manager Elodie Lize. My gratitude also goes to Professor Guillaume Ducrozet for making all the arrangements for this master thesis.

Last but not the least I would like to thanks my parent and wife for their sacrifices. Without their support it would have been impossible.

Abstract

In the framework of the completion of EMShip (Erasmus Mundus Double Master in Ship Design and Offshore Structures) Program, this master thesis was undertaken at LHEEA (Laboratory in Hydrodynamics, Energetics and Atmospheric Environment), a CNRS/Ecole Centrale Nantes research laboratory.

The purpose of this thesis is the estimation of the non-linearities associated with sea-keeping computation encountered in highly cambered waves. Linear methods like NEMOH developed for small displacements computations do not give good result. To estimate nonlinearity the weakly-nonlinear seakeeping code known as CN_WSC (Weak-Scatterer) was developed.

To quantify the non-linearities associated with highly cambered waves, a vertical cylinder was taken and it's motion response are calculated with CN_WSC (Weak-Scatterer) and similar calculations are done with linear code NEMOH. The motions calculated with both methods are compared and differences in the motion for highly cambered waves are illustrated as non-linearities were studied.

1   Introduction

For centuries, numerous methods and principles were adopted to understand the behaviour and calculate the forces exerted on the offshore structures. Last few decade, the efforts have been put in the area of the research and development of computational modelling . But these computational tools and methods are not precise and accurate enough to meet real scenario in the ocean. The reason behind these inaccuracies are due to various hypothesis and assumption adopted to solve these problem. The example of such method are linear potential solver to calculate the behaviour and the forces exerted on the these offshore structures. These are quick and computationally affordable but inaccurate enough to model real scenario of sea and body non-linearities. On the another hand methods such as fully non-linear model which is efficient and competent to model real scenario of sea and body non-linearities but the cost, computational time and skills requirements are massive.

   Therefore, weak-scatterer approach is the middle ground between above two method. It is quick, computational affordable and competent enough to model most of real sea and body non-linearity. The first approach on this model was made by Pawlowski [22] in 1991, where he proposed that perturbation potential is lower than that incident potential. So, the boundary condition of the free surface can be linearised around the incident wave field and forces are calculated by integrating the pressure over the immersed part of the body. A good amount of progress were made since and recent research on this approach goes back in 2012, when weak-scatterer non-linear code was developed at LHEEA laboratory of Ecole central Nantes, France.

   The objective of this thesis lies in the study of non-linearities through this approach of the potential flow theory. This was done through varying the numerical non-linearity such fixed body to free body, linear free-surface to non-linear free surface, body linearisation to exact-body and finally inclusion of the physical non-linearity as changing the steepness of wave from small to large. To study these non-linearity a vertical cylinder of dimension of radius $0.5m$ and draft of $2.0m$ was taken.

2   Literature review

A short literature review of various sea-keeping methods is essential to clearly identify the exact place of the weakly non-linear CN_WSC potential flow solver. In the last couple of decades, various methods have been evolved for compu-

tation of the sea-keeping behaviour of ships and offshore structures. Most of these methods are based on the potential flow model where fluid is assumed to be non viscous, incompressible and flow as irrotational. These sea-keeping methods show a good agreements between the theory and experiments and also show great compromise between accuracy and computational time.

2.1 Non-linearity

Even before going further to discuss about the the place of the non-linear solver, there is a need to introspect. If we talk about the ship and offshore structures, non-linearity present everywhere in the reality. No such linear system in realistic world. The ocean in which the ships travels doesn't produce linear and sinusoidal wave, neither the the response and the loads acting on ships.

For decades, the waves were assumed to be of small steepness to easily model it. Whereas fluid are also assumed to be non-viscous and flow to incompressible and irrotatinal to omit the associated non-linearity. Because it was easier to model and simulate the linear potential flow theory than viscous flow. Similarly the response and loads acting on the structures are assumed to be linear for the easier modelling, simulation and deal with lack of computing power of computers in the early decades.

But the recent decade arrived with the huge computing power such as super-computer, there lies an opportunity to exploit these computing power through modelling and simulation of non-linear system and try to understand the physics behind.

2.2 General Potential flow theory

Before going to discuss the different types of potential flow solver, it is pertinent to talk about the general background behind the potential flow theory. In this theory, fluid is assumed to be inviscid, so mathematically:

$$\mu = 0 \tag{1}$$

Since, flow is also assumed to irrotational. By the definition of irrotational flow, curl of the velocity of the fluid is null in the domain. Mathematically, it can be written as:

$$\nabla \times \vec{V} = 0 \tag{2}$$

Considering a potential function $\phi(x, z, t)$ a continuous function which satisfies the basic law of fluid mechanics i.e. conservation of mass and momentum

and flow to be based on the above assumption. As the fluid is assumed to be incompressible:

$$\rho(x, y, z, t) = \rho(constant) \tag{3}$$

Then, the continuity equation based on the conversation of mass states:

$$\frac{\partial \rho}{\partial t} + \nabla.(\rho \vec{V}) = 0 \tag{4}$$

Since, the condition of incompressibility states the time derivative of the density is zero and the density can be weed out of the divergence through division and the continuity equation of the incompressible system becomes:

$$\nabla.\vec{V} = 0 \tag{5}$$

Recalling, the vector identity for scalar potential function $\phi(x, y, z, t)$

$$\forall \phi \in R, \vec{\nabla} \times \vec{\nabla}\phi = 0 \tag{6}$$

Based on the Eq. 2 and Eq. 6,

$$\vec{V} = \nabla\phi \tag{7}$$

2.2.1 Laplace Equation

Substituting the Eq. 7 in Eq. 2 , it becomes:

$$\nabla^2\phi = 0 \tag{8}$$

The Eq. 4 ultimately called as Laplace equation.

2.2.2 Bernoulli Equation

It is derived from the momentum equation using the aforementioned hypothesis of potential flow theory and the equation becomes:

$$\rho\frac{\partial \phi}{\partial t} + \frac{1}{2}\rho V^2 + P + \rho g z = c(t) \tag{9}$$

To solve the equations in the fluid domain, one need to define a domain of resolution and the corresponding boundary conditions. These Boundary Conditions are derived from the natural limits of ocean such as the free surface (the moving interface between the ocean and atmosphere) and the bottom of ocean.

2.2.3 Kinematic free surface boundary condition

Kinematic free surface boundary condition: It states that velocity of the fluid normal to the free surface must be equal to the free-surface velocity in that direction. Mathematically defined as:

$$\frac{\partial \eta}{\partial t} = \frac{\partial \phi}{\partial z} - \nabla \phi . \nabla \eta \tag{10}$$

on $z = \eta(x, y, t)$

2.2.4 Dynamic free surface boundary condition

Dynamic free surface boundary condition : It states the pressure is constant at the free surface. Mathematically defined as:

$$\frac{\partial \phi}{\partial t} = -g\eta - \frac{1}{2}|\vec{\nabla}\phi|^2 + C(t) \tag{11}$$

on $z = \eta(x, y, t)$

2.2.5 Bottom Boundary Condition

Bottom is assumed fixed in time and defined by $z = -d(x, y)$. As the potential flow theory assume no viscosity and adherence condition led to slip/no flux condition through bottom [10] .

$$\frac{\partial \phi}{\partial z} + \nabla \phi . \nabla d = 0 \tag{12}$$

2.2.6 Solid Surface Boundary Condition

Due to inviscid nature of the fluid led to slip condition on the solid boundaries of normal n:

$$v.n = \frac{\partial \phi}{\partial n} = v^{Solid}.n \tag{13}$$

2.3 Boundary Integral Equation

The Laplace equation mentioned in the Eq. 4, is transformed into boundary integral equation (BIE) with Green's second identity [17]

$$\alpha(x_l)\phi(x_l) = \int_\Gamma [\frac{\partial \phi}{\partial n}(x)G(x, x_l) - \phi(x)\frac{\partial G}{\partial n}(x, x_l)]\partial \Gamma \tag{14}$$

Where G is the free-surface Green's function for fully- nonlinear solver and Rankine sources for Weak-Scatterer solver and α is the interior solid angle . In three dimensions, for a distance $r = x - x_l$, it can be written as:

$$G(x, x_l) = \frac{1}{4\pi |r|} \tag{15}$$

$$\frac{\partial G}{\partial n}(x, x_l) = \frac{1}{4\pi} \frac{r.n}{|r|^3} \tag{16}$$

2.4   Boundary Value Problems

The combination of the equations from Laplace Equation to all the boundary conditions with radiation condition becomes a set of equations represents for general non linear boundary value problems:

$$\begin{cases} \triangle \phi = 0 \\ \frac{\partial \phi}{\partial n} = \vec{V}\vec{n} \\ \frac{\partial \phi}{\partial n} = 0 \\ \frac{\partial \eta}{\partial t} + \vec{\nabla}\eta \vec{\nabla}\phi = 0 \\ \frac{\partial \phi}{\partial t} + g\eta + \frac{1}{2}(\vec{\nabla}\phi)^2 = 0 \\ \sqrt{R}(\frac{\partial \phi}{\partial \eta} - ik)(\phi - \phi_0) \to 0 \end{cases} \tag{17}$$

These equations need to solved in all the potential flow solver. Based on the hypothesis present in the solver, these equations need to be modified.

2.5   Types of Potential flow solver

2.5.1   Linear model

Linear model is the most simplified model as its name signify. In this model both the free surface and body non-linearities are simplified. In other words, the body are assumed to have small amplitude motion.

The perturbed components in this model are written in terms of Stokes series expansion [25] :

$$\phi^P = \phi^{P(0)} + \epsilon \phi^{P(1)} + \epsilon^2 \phi^{P(2)} + 0(\epsilon^3) \tag{18}$$

$$\eta^P = \eta^{P(0)} + \epsilon \eta^{P(1)} + \epsilon^2 \eta^{P(2)} + 0(\epsilon^3) \tag{19}$$

Each terms in the above equation depends on the problem of order of magnitude. The first order depict the fully linear problem whereas 2nd order depicts the quadratic terms. Another classical decomposition are also done based on the superposition principle so perturbed velocity potential is written as:

$$\phi = \phi^I + \phi^D + \phi^R \tag{20}$$

As shown, total velocity potential are decomposed into two parts, first ϕ^I which is known as incident velocity potential and ϕ^D as diffraction velocity potential which occurs when body is fixed and the incoming wave is present. Another is ϕ^R known as radiation velocity potential, when the body moves forcefully without the presence of incoming wave. The radiation velocity potential is further decomposed into its elementary quantities according to its (j) degree of freedom [16].

$$\phi^R = \sum_{j=1}^{6} \phi_j^R \tag{21}$$

The elementary problem of these velocity potential can be solved and global solution can be obtained through superposition. Hence, the radiation problem are solved for each frequency and direction of interest considering an harmonic motion. Then once hydrodynamics problem are solved, a hydrodynamics database can be created with added mass, damping term and exciting forces.

$$([M] + [\mu])\ddot{X}(t) + [\lambda]\dot{X}(t) + ([K_H] + [K_A])X(t) = Re[(F_I + F_D)e^{-i\omega t}] \tag{22}$$

Where [11],

- $[M]$ and $[K_H]$ are mass and restoring force matrix depends on the body characteristics (more precise geometry and mass distribution).

- $[K_H]$ is the mooring system matrix.

- $[\mu]$ and $[\lambda]$ obtained from solving the radiation problems in NEMOH.

- F_I and F_D are the incident and diffraction forces.

Later these frequency dependant quantities can be used to calculate the structure response. Even time domain simulation is possible with the help Cummin's equation [9]. Based on the Stokes series expansion, the second order problem can be also be defined and new set of frequency -dependent coefficient known as quadratic transfer function can also be created [23].

The first and 2nd order frequency domain model are widely used in the industries and laboratories to solve the problem related to ship resistance, manoeuvring and sea-keeping. Various sea-keeping computational softwares such Diodore [2], Hydrostar [3], NEMOH [4], WAMIT [5], ANSYS Aqua [6] are based on the linear model. But for large wave motions, the small amplitude based model have huge limitations.

Another important parameter need to talk about is mesh. In this model, the body boundary condition are linearised about the mean position of the bodies. The pressure is also integrated over the fixed mean wetted body surface. Therefore, mesh of the body is fixed. On the another side, the linearisation of the free surface boundary condition is also applied that lead to totally still mesh.

2.5.2 Body-exact model

This model is based on the simplification of free surface condition. This simplification was maintained with linearising the free surface condition around the mean free surface elevation $z = 0$.

Advantages associated with this model are as follows:

- Due to linearisation of free surface condition free surface mesh remain planner, which create a faster mesh convergence

- Faster mesh convergence leads to reduction in the computational time.

- Mean surface elevation leads to easier integration of pressure.

Similarly it have major drawbacks that this methods is only consistent when wave steepness is small. Based on this body exact method, sea-keeping analysis was performed by R. A. Watai [24].

2.5.3 Weakly nonlinear hypothesis

The weak-scatterer hypothesis was first developed by Jacek S. Pawlowski and Don W. Bass around 3 decades back in 1991 to perform the numerical simulation of large ship motions in the heavy seas. The main assumptions they took are described in their words [21]:

"The disturbance induced by the moving ship in the wave flow is considered to be of smaller magnitude than the wave flow quantities which are proportional to the wave height, but at least of the same magnitude as the wave flow quantities

proportional to the square of the wave height. This assumption, explained here in simple terms, is called the weak scatterer hypothesis."

So, the scattered wave components from the body are assumed to be much smaller or weaker than the incident wave. That's why this theory are named as weak scatterer. In J S Pawlowski words to Dr. Martin, he mentioned " Formally a scatterer is weak if the the (disturbances) waves generated by the scatterer are sufficiently small in comparison with the ambient wave field." his assumption is nothing but the extension of the Froude-Krylov hypothesis which currently used as paradigm that the presence of the ship does not change the pressure distribution in the propagating wave.

He also highlighted a number of physical circumstances under which the this formal requirement is satisfied. For instance a sufficiently deeply submerged body of any shape becomes a weak scatterer, as does a slender ship advancing in bow waves. In other words, the weak scatterer hypothesis is applicable when the ships moves compliantly with the waves and this usually happens for a free floating ship which operates in the steep waves of a length and height comparable to the ship's dimensions.

This theory, according to him is applicable in the case of :

- Large Body motions

- Steep wave

Similar to other theory, this hypothesis too decompose the velocity potential and the wave elevation into an incident components and a perturbed components.

As the main objective of this Master thesis is validation of Weak-Scatterer nonlinear potential model with experimental results, so the more details about this model are described in the later sections.

2.5.4   Fully non-linear model

When the potential flow theory directly applied, it known as fully non-linear theory. Here bodies and the free surfaces are meshed on the their real position and the pressure is integrated over the instantaneous wetted surface. So, it is the most accurate theory based on the potential flow approximation. It is widely used to simulate wave propagation.

But the problem with method exist during fluid- structural simulation. Although it is possible to express the boundary conditions on the bodies and the free surface at exact position. But it necessary to re-grid the mesh i.e. firstly

update the position of he mesh and second prerequisite requirement is to keep a good quality mesh which deformed by the waves and bodies. The other disadvantages exist with fully non-linear theory are listed below[25] :

- In the case of surface-piercing bodies, to avoid sawtooth instabilities, smoothing techniques are needed.

- For any translational and rotational motion,it is very difficult task to compute the intersection curves between the free surfaces and the bodies.

- Artificial damping coefficient are required on the free surface to avoid the reflection of the perturbed waves at the numerical boundaries. While fully describing the free surface in such cases , wave breaks and simulations stops.

- Space discretization of mesh should be small enough to simulate all the perturbed waves generated due to presence of the bodies.

Due to above challenges exist in the fully nonlinear models which makes it numerically arduous. Hence to reduce the complexities involve in the fully nonlinear approach, there have been a clarion call for the development the other nonlinear model and weakly nonlinear model is one of them.

2.5.5 Summary

Below Fig. 4 summarize the main differences between the various potential flow theories: Since untill now only three methods/approaches have been used for sea-keeping motion computation of ship and offshore structures: a frequency -domain model, a linear time domain model and a fully non-linear potential flow model. But this weakly non-linear model which is based on the weak scatterer hypothesis is applicable for simulation of marine operations where interactions of several bodies are involved and possibly have a large motion. In that case fully linearisation of body interaction made in the case of a linear potential flow based solver is not applicable because it is too restrictive in nature. Moreover, the consideration of frequency domain solver is out of the question because it is limited to linear potential theory. In such cases, weakly non-linear theory, no hypothesis is needed about the small body amplitude (linear model), neither the unsteadiness of the flow (frequency domain model) nor the small wave steepness (Body exact model, Non-linear Froude-Krylov model, Linear time domain model and frequency domain model). Compared to a fully non-linear approach, it is

expected to have more stable simulations and faster. But some non-linear effects like wave drift, hydrodynamic impact may be underestimated.

	NL	WSC	BE	NFK	LTD	FD
Decomposition	ϕ or $\phi = \phi^I + \phi^P$	$\phi = \phi^I + \phi^P$	$\phi = \phi^I + \phi^P$	$\phi = \phi^I + \phi^D + \phi^R$	$\phi = \phi^I + \phi^P$ or $\phi = \phi^I + \phi^D + \phi^R$	$\phi = \phi^I + \phi^D + \phi^R$
Assumptions	ϕ	$\phi^P \ll \phi^I$	$\epsilon \ll 1$	$\begin{cases}\epsilon \ll 1\\ A_m \ll 1\end{cases}$	$\begin{cases}\epsilon \ll 1\\ A_m \ll 1\end{cases}$	$\begin{cases}\epsilon \ll 1\\ A_m \ll 1\\ \text{Steady state}\end{cases}$
Meshed free surface	$z = \eta(x,y,t)$	$z = \eta^I(x,y,t)$	$z = 0$	$\begin{cases}z = \eta^I(x,y,t) & \text{for HS and FK;}\\ z = 0 & \text{otherwise.}\end{cases}$	$z = 0$	$z = 0$
Mesh body surface	$S_B(t)$	$S_B(t)$	$S_B(t)$	$\begin{cases}S_B(t) & \text{for HS and FK;}\\ S_B(0) & \text{otherwise.}\end{cases}$	$S_B(0)$	$S_B(0)$
Time	$\mathcal{O}(1\text{ week})$	$\mathcal{O}(\text{Days})$	$\mathcal{O}(1\text{ day})$	$\mathcal{O}(1\text{ h})$	$\mathcal{O}(1\text{ h})$	$\mathcal{O}(1\text{ h})$

Table III.1 – Main differences between several potential flow theories. NL: Fully nonlinear, WSC: Weakly nonlinear based on the weak-scatterer hypothesis, BE: Body exact approximation, NFK: Nonlinear Froude–Krylov, LTD: Linear time–domain, FD: Frequency–domain. A_m denotes the body motion amplitude. HS and FK represent the hydrostatic and Froude–Krylow loads.

Figure 4: Different Models comparison[25]

2.6 *Weakly nonlinear model based on the Weak-Scatterer hypothesis*

2.6.1 Historical Developments

Aforementioned, this hypothesis was introduced by J. Pawloskwi and Bass in 1990. To perform time domain computation of large ship motions in heavy sea, he accounted that weak scatterer assumption was used before in (Newman, 1970) as reported in (Salvesen, 1974) in an investigation of hydrodynamics loads on submerged bodies in (Salvesen,1974) for simplification of the expression for second order hydrodynamics loads induced on the conventional surface ships.

It also account that this assumption was made in the context of "strip theory" (Salvesen, Tuck and Faltinsen, 1970) and is justified for slender ships operating at normal speeds in head and bow waves. But if we look on the present hypothesis, it is not limited as similar to former but it is extended to compliant motion of ships in waves and applicable to the modelling of large ship motions. This the describe the major difference between the weak scatterer assumption between (Salvesen, Tuck and Faltinsen, 1970) and (J. Pawloskwi and Bass, 1990).

So, Pawlowski et. al [20],[21] firstly applied this method to Series 60 and Trawler to validate numerical results with experiments data in Small amplitude and steep regular wave. He observed an good agreements with experiment to the numerical results produced through this model. Through this conclusion, he validated the hypothesis/assumption.

Few years later in 1994, Lin et al [18], supplemented an study on this hypothesis through development of a time domain solver called LAMP -4. This numerical solver is a part of LAMP porgram (Large Amplitude Motion Program) used for the computation of the motion and load of a ships operating in the extreme weather conditions. LAMP-4 is the revised version of the LAMP-1 ,LAMP-2 and LAMP-3 which are based on the linear, nonlinear Froude-Krylov and large displacements models respectively.

D.C. Kring et al at MIT, developed another multi-level potential flow based numerical tools known as SWAN (Ship Wave ANalysis). It have different variants similar to LAMP, known as SWAN-1, SWAN-2 and SWAN-3 applicable for a linear frequency domain code, a linear frequency domain code with linear or nonlinear Froude-Krylov loads and a time domain code based on the weak scatterer hypothesis respectively. He has also used SWAN-4 (based on weak-scatterer) hypothesis for Series 60 and a Snowdrift moving with head seas and compared with SWAN-2 (linear wave theory) and found that both the methods are comparable and have good agreements. Actually the extension of SWAN

to weak-scatterer hypothesis based SWAN-4 are done by Huang [13] in his Ph.D. thesis. He also accounted for the comparison between linear and weak-scatterer hypothesis with container ship in head seas.He also noticed in his thesis that while comparison to SWAN-4 to SWAN-2, for small wave slope, the weak scatterer method converge to the linear theory . But as soon as the incoming waves becomes steeper, the disparity between the linear and weakly-scatterer hypothesis increases.

The comparison of the different variant of SWAN (SWAN 1, SWAN 2, SWAN 3, and SWAN 4) are compared by Grigoropolus et. al. [12] to experimental data in 2011. He compared these variants of SWAN model with different types of Ships such a s Series 60, a refer and a ROPAX. He concluded that both SWAN 1 and SWAN 2 gave robust numerical results to each load cases but addition of Non-linear Froude-Krylov loads due to SWAN-3 added better accuracy to the predictions. Whereas using SWAN-4 gave quite different results which is very different from experiments.

After development of the different version of LAMP and SWAN, a third numerical tool is developed by Y. Kim et.al. at Seoul National University, Korea. It is known as WISH (Wave-induced loads and Ship motion) and used the weak-scatterer hypothesis. Similar to LAMP and SWAN, 3 version of the WISH has been developed known as WISH 1, WISH 2 and WISH 3, these are based on the linear time domain code, linear time domain-code with nonlinear Froude-Krylov load and a time domain code based on the weak-scatterer hypothesis respectively.

Kim et. al [14] in 2009, compared the SWAN-4, WISH 3 (both Weakly-Scatterer hypothesis based) and experimental data for a Series 60 and Container-ship and mentioned that they all gives comparable results although formulations are different. Other comparison was made with all 3 versions of WISH for containership in head sea to experimental data and results was found comparable. Lastly, he concluded that results were best using weak-scatterer formulations especially in rough sea.

Application to Weakly-scatterer hypothesis was firstly extended to non-ship like structure by Bretl [7]. It was used in the study of Wave Energy converter made of floating rigid hemisphere coupled with a planner pendulum in his Ph.D. work.

2.6.2 Recent Advancements

Recent advancements in the area of the weakly-scatterer nonlinear code are based in the chronology of its potential flow based solver development at LHEEA

laboratory of Ecole Centrale de Nantes in 2012.

After development of WS_CN potential flow solver at ECN, the first development is "development of a numerical tool based on the weak scatterer (WS) approximation for the study of Wave Energy Converters in the Large motion" by Lucas Letournel in his Ph.D. thesis [16]. Here, firstly he compared the weak_scatterer theory to the linear approach in the case of the diffraction of regular wave for a fixed sphere and it was noted that for small steepness regular wave case the hydrodynamics loads calculated through both the methods matches but for high steepness waves differences are drastic.

Later, Chauvigne [8] extended Letournel work a bit further, he used the WS_CN to surface piercing body in the case of arbitrary motion. To generate the total mesh or regenerate the body mesh, an advanced front method was used. Studied was made for diffraction of regular wave by either a bottom fixed or truncated surface piercing body. Linear and fully non-linear theories and experimental data for the maximum run-up around the cylinder are compared . Since the case being highly non-linear, so finally weakly non-linear, fully non-linear and experimental data are compared and it was found that for the case of two configuration (fixed bottom and surface piercing) weak-scatterer model was in line with fully non-linear theories and experimental data in the bow side but over estimated the maximum in the lee side. He also extended the approach for evaluation of the radiation of the truncated cylinder. Similar to Letournel [16], it was mentioned that, WS_CN matches the linear theory for regular wave case but differences occurs in the case of high amplitude wave.

Then, Wuillaume [25], carried forward the Chauvigne [8] in his Ph.D work. He extended the WS_CN to large deformation of the free mesh surfaces in the case of the multi-body simulation. Validation of the forced motion was presented with experimental data. It was noted that experimental data and weak scatterer gave comparable results for both hydrodynamics loads and the wave elevations. The analysis of weak-scatterer hypothesis was also done through the comparison drawn between body-exact approximation and fully linear approximation. It was concluded that when the wave steepness was small, the body-exact model gave good results compared to experiment. Nevertheless when the wave steepness and free surface non-linearities were increased, differences seen between weak-scatterer and body exact approaches.

So, above all three Ph.D. thesis emphasis a need for Wave-scatterer non-linear solver to get the exact solution in the case large wave motions.

2.6.3 Assumptions and governing equations

Similar to general potential theory discussed in the Section 2.2, the assumption are in the weak-scatterer sea-keeping theory as follows which were discussed by [25]

- First and foremost, the validity of weak-scatterer hypothesis.

- Second, the rigidity of the floating and submersed bodies. In this thesis only floating case of the cylinder was considered.

- Third, the assumption of the tri-dimensional, unsteady and potential flow. The unawareness of the surface tension.

- Fourth, the flat sea bottom, single valued free surface elevation to avoid wave-breaking and nullity of the pressure above the free surface.

To validate these assumptions and governing equations, a fluid domain (D) was defined which has a boundary (D_S), constituted of the free surface (D_{FS}), the wetted body surface(B_S) and the numerical tank surface which includes the sea bottom (SB) as shown in the Fig. 5
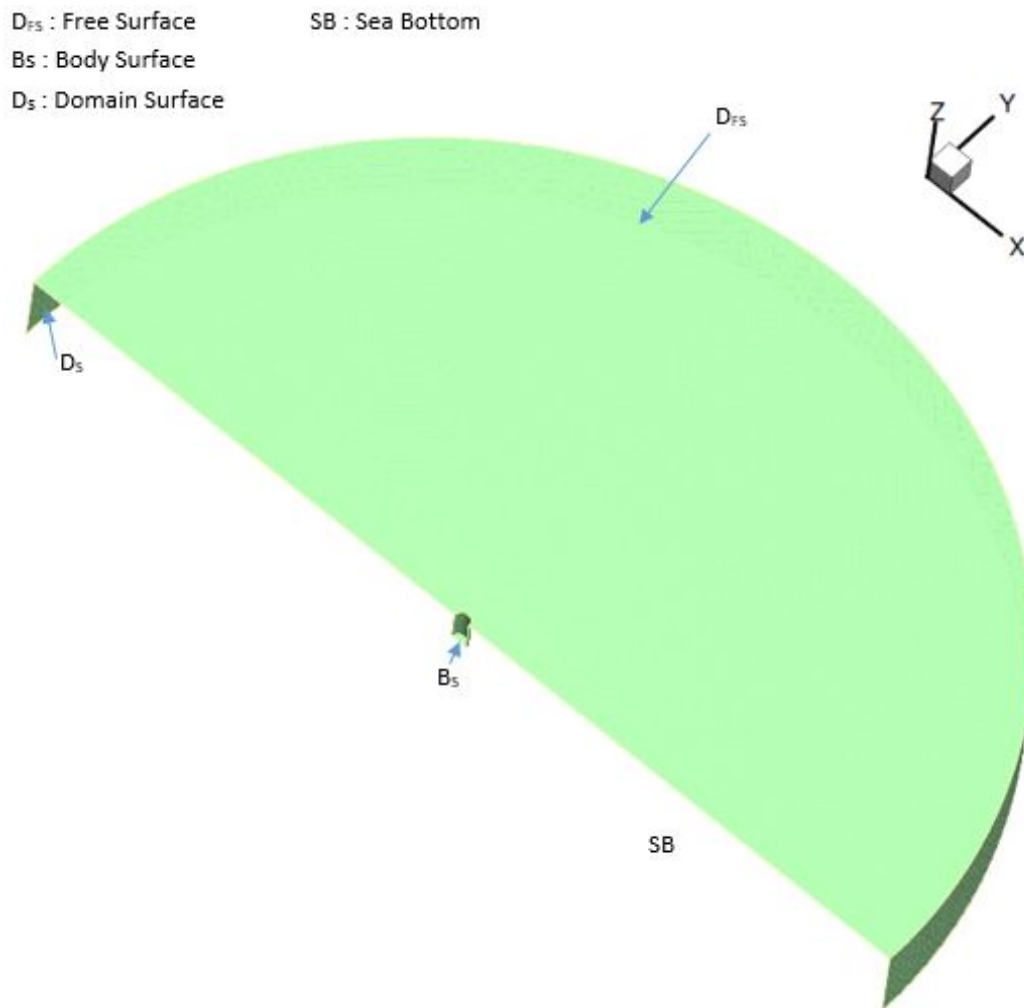
Figure 5: Fluid domain

Similar to the other model, the velocity potential and the wave elevation are decomposed into an incident and perturbed components as follows:

$$\begin{cases} \phi = \phi^I + \phi^P \\ \eta = \eta^I + \eta^P \end{cases} \tag{23}$$

Where, first term is known as incident components and known in advance. Whereas the second term is known as perturbed and unknown. As the weak-scatterer hypothesis assume, perturbed components are smaller compared to Incident terms as defined below:

$$\begin{cases} \phi^P \ll \phi^I \\ \eta^P \ll \eta^I \end{cases} \tag{24}$$

Based on the above assumptions, following simplicities arise as explained by [25]:

- The free surface boundary equations are linearised around the free surface elevation $z = \eta^I(x, y, t)$. So, the free surface nonlinearites are simplified.

- Opposite to full non-linear approach, this surface is known.

- Since, the perturbed items are small. so, it is not necessary to mesh these waves and only incident waves needs to be meshed.

- The pressure is integrated over the instantaneous wetted waves body surface are only delimited by the incident waves.

- Weak-scatterer hypothesis led to possibilities to use large spatial desensitization and therefore reduce the CPU time.

- This solves doesn't take any assumption about the body nonlinearities.

- It also comes with big disadvantage that this potential solver is only adapted to slender surface piercing bodies with and without forward speed and immersed bodies.

Pierre-Yves Wuillaume [25] also listed the equation used in the Weak-scatterer hypothesis as follows based on the decomposition Eq.(11).

$$\begin{cases} \triangle \phi^P = - \triangle \phi^I & \text{in the fluid domain D} \\ \frac{\partial \eta^P}{\partial t} = -\frac{\partial \eta^I}{\partial t} - \nabla \phi^I . \nabla \eta^I - \nabla \phi^I . \nabla \eta^P - \nabla \phi^P \nabla \eta^I - \nabla \phi^P . \nabla \eta^P \\ \quad + \frac{\partial \phi^I}{\partial z} + \frac{\partial \phi^P}{\partial z} \\ \frac{\partial \phi^P}{\partial t} = -\frac{\partial \phi^I}{\partial t} - \frac{1}{2} \nabla \phi^I . \nabla \phi^I - \nabla \phi^I . \nabla \phi^P - \frac{1}{2} \nabla \phi^P \nabla \eta^P - g(\eta^I + \eta^P) \\ \frac{\partial \phi^P}{\partial n} = -\frac{\partial \phi^I}{\partial n} + v^{Solid} \\ \frac{\partial \phi^P}{\partial n} = 0 & \text{on the numerical tank walls} \\ \phi^P \xrightarrow[r \to +\infty]{} 0 \\ \eta^P \xrightarrow[r \to +\infty]{} 0 \end{cases} \tag{25}$$

2.6.4   Numerical Implementations

2.6.4.1   Discretization

Linear triangular elements is used via an isoparametric parametrization which describe the geometry as well evaluations of the unknowns[17]:

$$f(x) = f(x_1) + u(f(x_2) - f(x_1)) + v(f(x_3) - f(x_4)) \tag{26}$$

$$= f(x_cg) + \nabla_s(f).x_{cg}x \tag{27}$$

Where, x_{cg} is the center of gravity of the triangular elements (x_1, x_2, x_3) and $\nabla_s(f)$ indicates the surface gradient of f and can be calculated with the derivatives of f along u and v. Then the integrals in the Boundary Integral Equation of Section 2.3, can be separated into two terms. The analytical solution for the single integral with Rankine sources were developed with a decomposition on each side of the triangular panel [16].

3   Methodology

As the main objective of this thesis to understand the non-linearities associated with the test cases with change in the numerical and physical non-linearity. To perform the simulations, a cylinder as shown below was taken of following dimensions:

Figure 6: Geometry of the cylinder
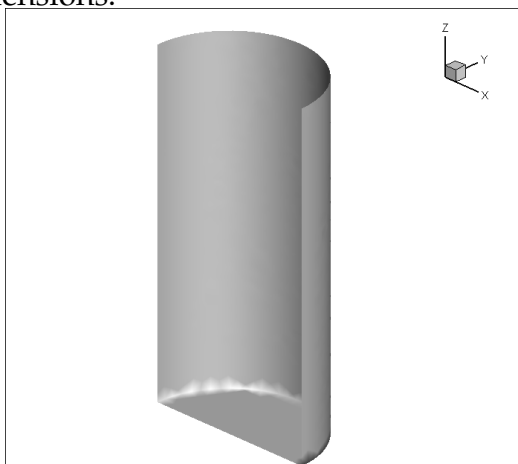
Parameters	Values	Unit
Radius	0.5	m
Draft	2.0	m
Mass	1610.066	Kg

Table 1: Parameters of the cylinder

First of all, convergence study was performed for both solvers NEMOH and WS to understand the converged mesh sizes which can be used for future

computation and comparison.

Once the convergence was completed, the sea-keeping test cases were divided into various section depending on the fixed or free body, low steepness or high steepness, linearised or non-linearised free surface and linearised or non-linearised body.

- Small/High Steepness (Physical non-linearity)

    - Fixed/Free body(Numerical non-linearity)

        * Linearised/Non-linear Free Surface
        * Linearised/Non-linear Body Motion

The computation of these cases were started with test case which had less complexities and took less computational time. The test case of linearised free surface and body motion for fixed body with low steepness of 0.45 % was the least complex and computational. The result obtained from this test case were compared with result obtained linear solver NEMOH to validate in the Section 4.3.1.2. Once the result were validated, the numerical non-linearity were added, just as non-linearising the free surface and body with the fixed body case. Then the result obtained from for this case were compared with the fully linear test case in Section 4.3.1.3.

In the next test case, the body were freed from fixed case and simulation were performed with linearised free surface and body motion in Section 4.3.2.3. Although this test case were not relevant much because free body case with fixed Free surface and body non-linearities is contradictory. So, later test cases associated with free body case chosen based on the only free surface test cases and fully non-linear free surface and body test cases. Although the free body test case with linearised free surface didn't work with due to instability in simulation so later test case in free body case only considered for non-linear free surface and body.

Then, the test cases were performed with highly complex non-linear free surface and body motion with higher steepness of 5 % as follows. Noting that In this thesis, % steepness are defined as follows

$$\%steepness = \frac{a}{\lambda} \times 100 \qquad (28)$$

Where, a = amplitude of the wave and λ = wavelength of the wave

4 Discussion of Results

4.1 Convergence analysis in WS

The convergence is important part in computational mechanics involved with meshes/elements/panels, because these affect the accuracies and of the results with refinement.

So, to understand the accuracies of the Froude-Krylov and diffraction forces, it was requisite to perform convergence analysis. This convergence analysis will give the convergence mesh sizes required during launching simulations and of-course the converged Froude-Krylov and diffraction forces which can be later used to understand non-linearities.

To perform convergence analysis, $dx1$(the panel size for numerical tanks walls and at the outer boundary of the free surfaces) was refined from 3 m to 0.4 m. On the another side $dx3$ which was panel size in meters at the immersed sharp edges of the bodies was varied from 0.2 m to 0.05 m and kept equal to $dx2$. The mesh size used for weak scatterer simulations were not optimum and efficient in nature. The $dx1$, $dx2$ and $dx3$ used in the input files of are 3 m, 0.2 and 0.2 m respectively. Note that $dx1$, $dx2$ and $dx3$ denote the mesh sizes of free surfaces as represented in the figure 7. So, the convergence analysis need to perform with reference to number of elements of the free surfaces during simulations to get more closer result with NEMOH.

From the above table 2, it can be seen that when the pannel sizes were refined from 3 m to 0.4 m for $dx1$ and 0.2 to 0.05 m for $dx2$ and $dx3$, the amplitude of Froude-Krylov force was increased from 3.810 N to 4.4246 N. Whereas diffraction force was decreased from 2.064N to 1.854N. To appreciate the convergence better, % Relative difference between the forces of consecutive mesh sizes were plotted below.
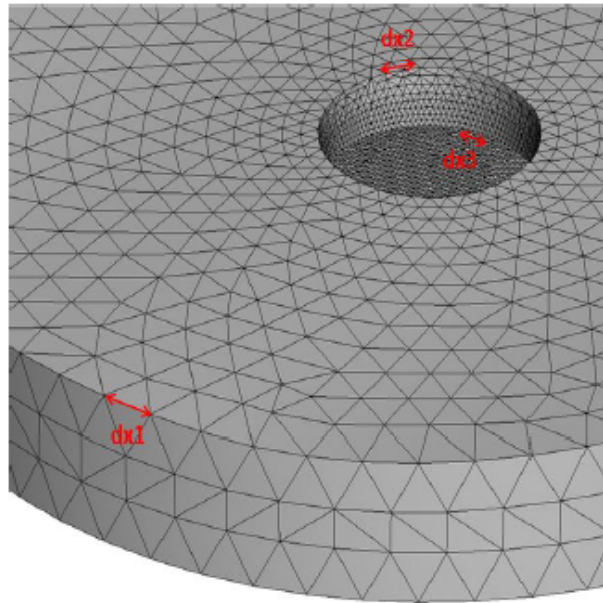
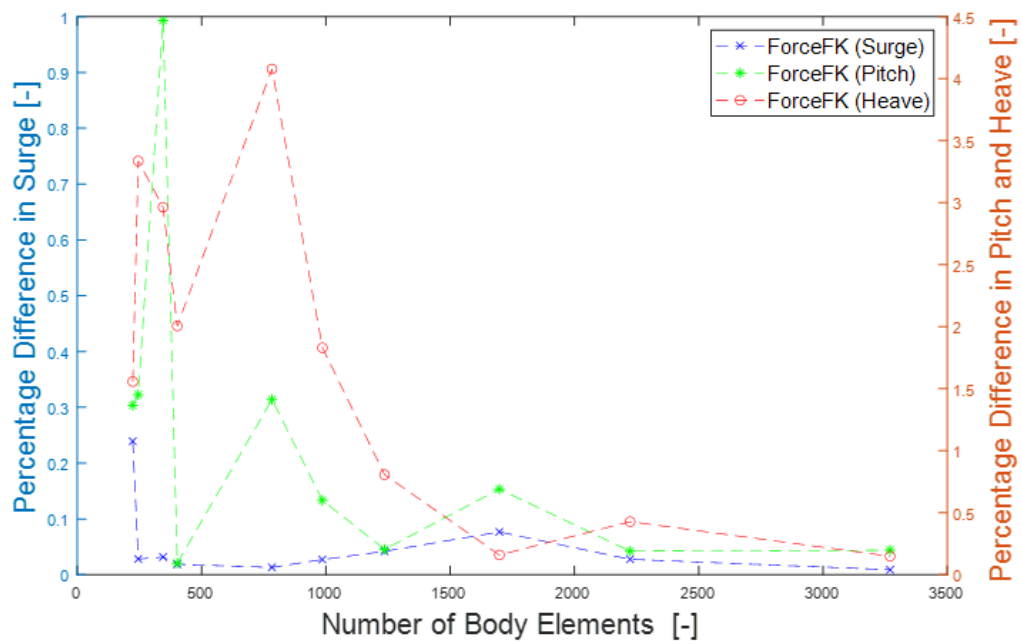**Figure 7:** Free surface mesh size (dx1, dx2 and dx3 representation [26]

Figure 8: Rel.% diff ForceFK Ampl

Table 2: Convergence Analysis for heave motion in WS

dx1	dx2 = dx3	No of Ele- ments	CPU time(s)	CPU time(h)	ForceFK Ampl.	Rel.% diff ForceFK Ampl.	ForceFd Ampl.	Rel.% diff ForceFd Ampl.
3	0.2	1371	130.83	0.04	3.810		2.064	
2.9	0.19	1510	185.80	0.05	3.869	1.56	2.645	28.14
2.75	0.18	1607	218.49	0.06	3.999	3.34	3.699	39.86
2.5	0.15	2083	407.92	0.11	3.880	2.97	1.657	55.21
2.4	0.14	2256	488.61	0.14	3.958	2.01	1.743	5.23
2	0.1	3608	1318.09	0.37	4.119	4.08	1.385	20.58
1.5	0.05	8773	10130.54	2.81	4.246	3.08	1.529	10.42
1	0.1	10117	8971.16	2.49	4.119	2.99	1.860	21.66
0.75	0.05	21521	75103.94	20.86	4.246	3.08	1.819	2.19
0.7	0.05	23755	90535.43	25.15	4.246	0.01	1.872	2.92
0.6	0.05	30324	165710.07	46.03	4.246	0.01	1.854	0.99
0.4	0.05	34484	184350.73	51.21	4.246	0.00	1.861	0.38
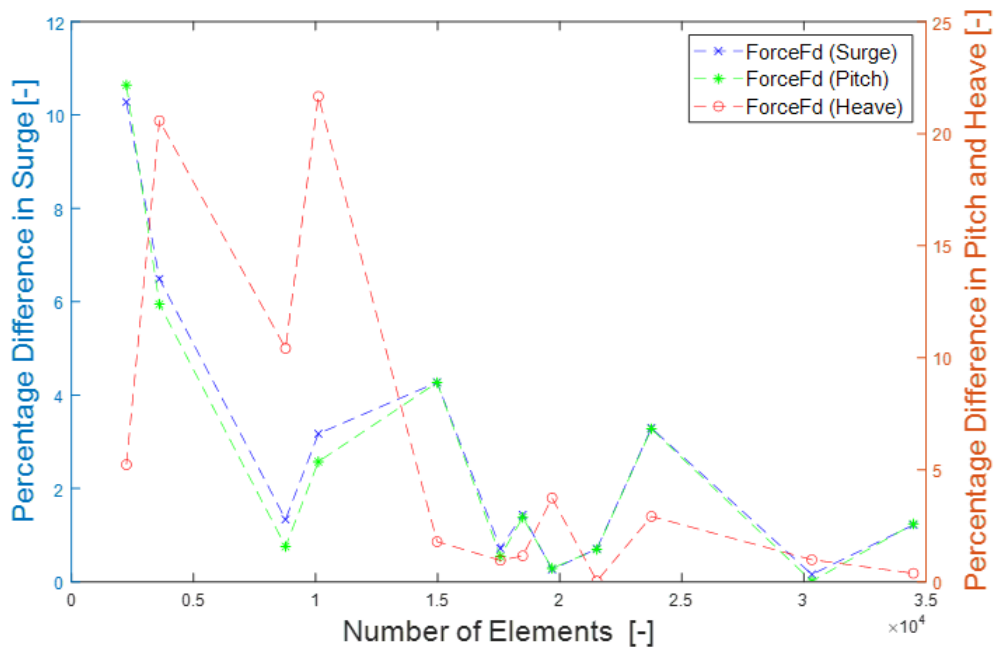
Figure 9: Rel.% diff ForceFd Ampl

From Fig. 8, it can be seen that relative % difference of Froude-Krylov forces were decreased from 1.56 % for (panel size $dx1 = 3$ m and $dx2 = dx3 = 0.2$m) to 0.01% for (panel size $dx1 = 0.40$m and $dx2=dx3=0.05$m) which was close to zero.

On the another hand, From figure 9, it can be seen relative % difference of diffraction forces too were decreased from 28.14 % for (panel size $dx1 = 3m$ and $dx2 = dx3 = 0.2m$) to 0.99% for (panel size $dx1 = 0.40m$ and $dx2 = dx3 = 0.05m$) which is close to 1%. It indicate that the mesh was converged for panel size $dx1 = 0.40m$ and $dx2 = dx3 = 0.05m$. But the converged panel sizes which selected were $dx1 = 0.75m$ and $dx2 = dx3 = 0.05m$, due to following reasons:

- The computational time required for panel size $dx1 = 0.40m$ and $dx2 = dx3 = 0.05m$, requires around 112 Hrs which is close to approximately 5 full day-night computational time. So, it was highly computational expensive.

- Important was to get an accurate results but the simulations should be computationally reasonable. So, the chosen converged panel sizes needed to be a trade off between the accuracy and computational reasonableness. The chosen converged panel size $dx1 = 0.40m$ and $dx2 = dx3 = 0.05m$ which was equivalents to around 21500 elements takes around 20.86 hrs of CPU time and have percentage difference for Froude-Krylov forces is 3.08 % and for diffraction forces are 2.19 % . It was reasonable compared to 112 hrs of computational time taken by the finest mesh listed . Note here, CPU time is not equal to real computational time took during simulation.
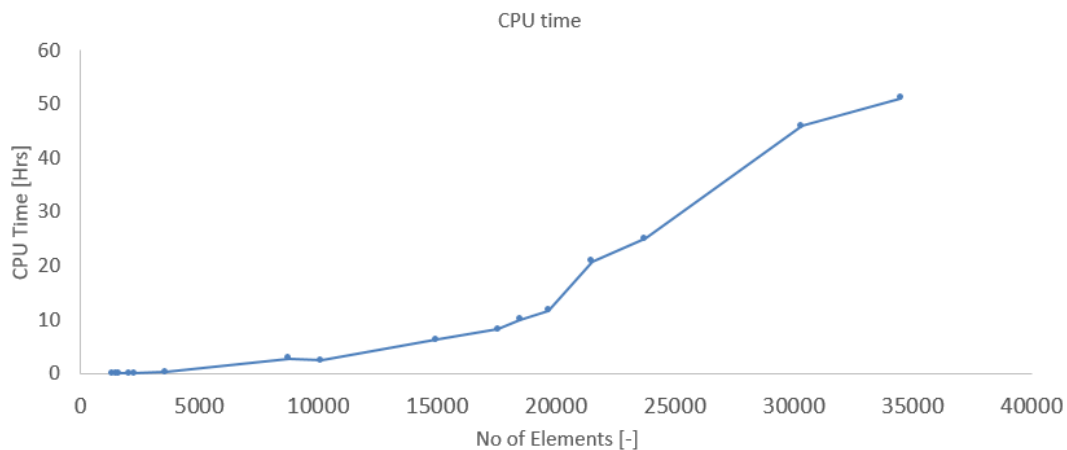

Figure 10: CPU Time in hrs

4.2   *Convergence analysis in NEMOH*

Based on the similar analogy as convergence analysis in WS, convergence analysis was performed during simulation of the cylinder in NEMOH. It should be noted that the geometry and dimensions of the cylinder were kept same. Frequency and the water depth too were kept same as 3.74 rad/s and 5 m respectively.

To perform the convergence analysis here, target panels were varied from 100 to 2000. In this master thesis, NEMOH panels size were limited to 2000. Then for every target panels, the simulations were performed and the Froude-Krylov force, diffraction forces, radiation forces, damping coefficient as well as added mass coefficient were calculated and tabulated below:

Table 3: Convergence Analysis for heave motion in NEMOH

Target panels	Exact No of panels	ForceFK Ampl.	Rel.% diff ForceFK Ampl.	ForceFd Ampl.	Rel.% diff ForceFd Ampl.	Damp. Coeff. [B]	Rel.% diff[B]	Added Mass	Rel.% diff CM
100	90	4.2088		1.9581		2.411		259.004	
250	225	4.2539	1.072	2.5586	30.667	2.378	1.393	257.365	0.633
400	361	4.2626	0.205	1.9378	24.263	2.360	0.761	255.872	0.580
800	756	4.2707	0.190	1.9272	0.547	2.391	1.321	254.368	0.588
1000	930	4.2722	0.035	1.9231	0.213	2.398	0.280	253.423	0.372
1600	1443	4.2741	0.044	1.9197	0.177	2.428	1.253	253.084	0.134
1800	1638	4.2747	0.014	1.9183	0.073	2.427	0.024	252.715	0.146
2000	1848	4.2749	0.005	1.9177	0.031	2.432	0.214	252.668	0.019

Now, to appreciate the convergence better, relative percentage differences were evaluated for all the forces, added mass and damping coefficient and plotted below.
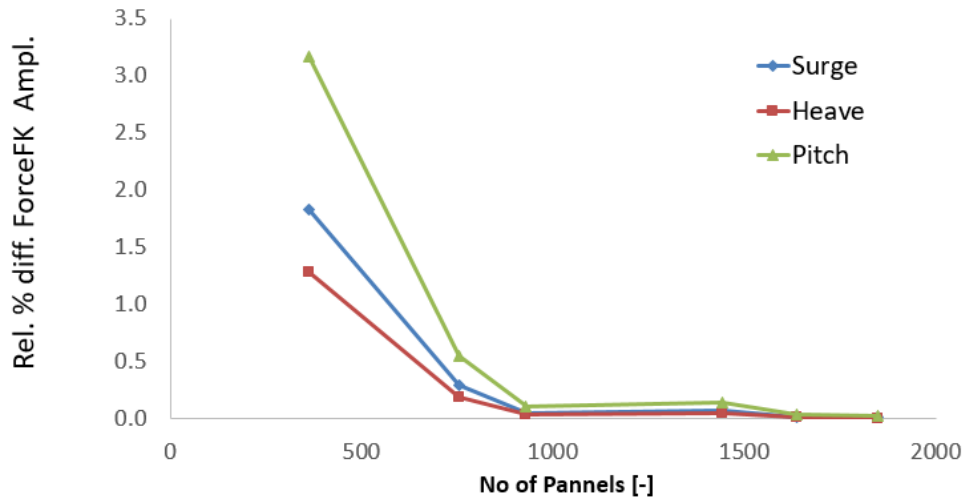
Figure 11: Rel.% diff ForceFK Ampl in NEMOH

From the Fig. 11, it can be seen that for surge motion of the cylinder, the relative percentage difference in Froude-Krylov force was 1.83 % for panel size of 361 and it was reduced to 0.012 % for panel size of 1848 which is close to 0. For heave motion and pitch motion similar behaviour can be seen.
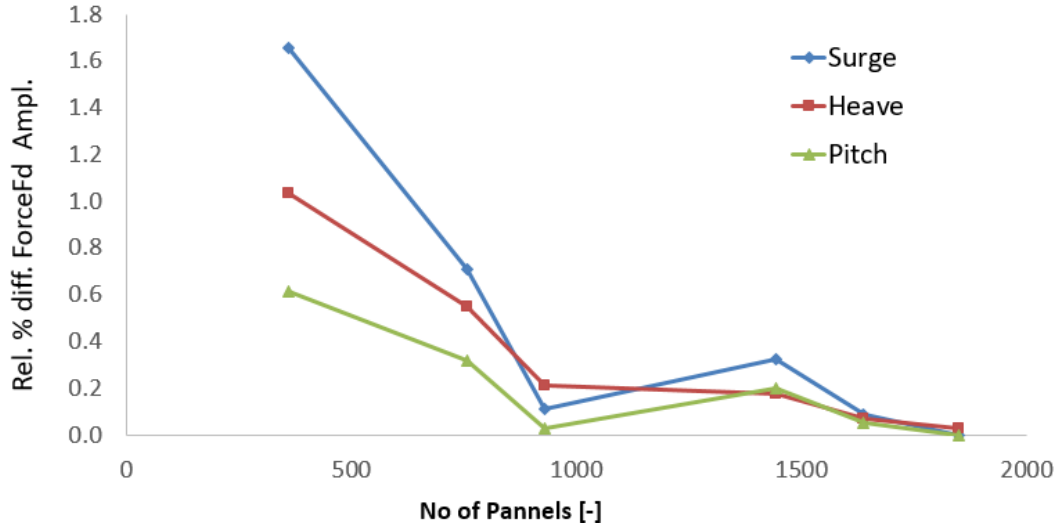

Figure 12: Rel.% diff ForceFd Ampl in NEMOH

Now if we follow for diffraction forces exerted on cylinder in NEMOH in Fig. 12, the relative percentage diffraction force amplitude was 1.656 % panel size of 361 and it was reduced for panel size of 930. But it shown a bit abnormality and

increased for panel size of 1443 and then it decreased to zero for panel size of 1848.

For heave motion, the relative percentage difference of diffraction Force amplitude was 1.037 % for panel size of 361 and it was reduced to for panel size of 756 and kept on reducing. Whereas for pitch motion, it was shown similar behaviour as surge.
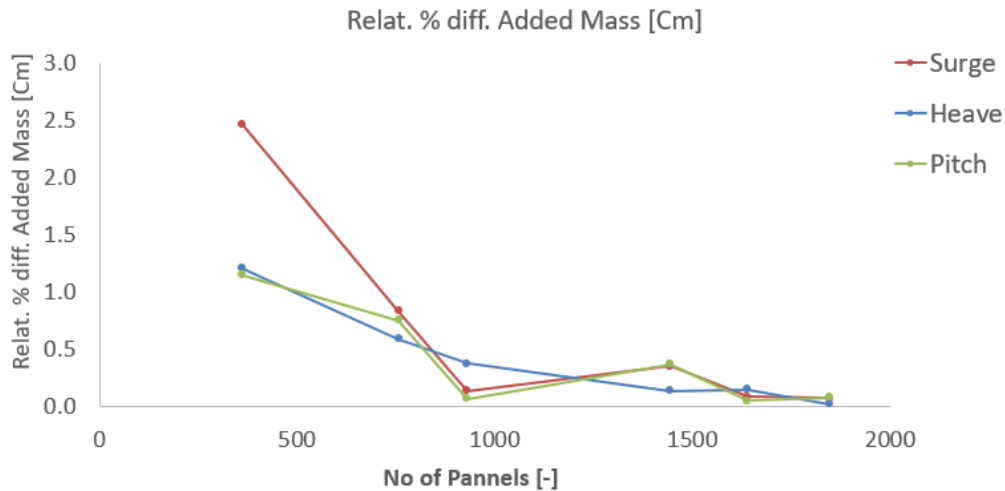

Figure 13: Rel.% diff Added Mass Coeff. in NEMOH

In Fig. 13, the plot for the relative percentage difference in added mass for was shown. From the figure, it shown that in surge for initial panel size of 361, it was 2.46 % and and it was reduced for panel size of 930. But it shown a bit abnormality similar to diffraction force amplitude and increased for panel size of 1443 and then it decreased for panel size of 1848. In heave, the relative % difference in added mass was 1.209% for initial panel size of 361, then it reduced to for panel size of 1443, very slight increase was seen for panel size of 1638 and finally reduced back to 0.079 % for panel size of 1848. Whereas for pitch motion, it shown similar behaviour as surge.
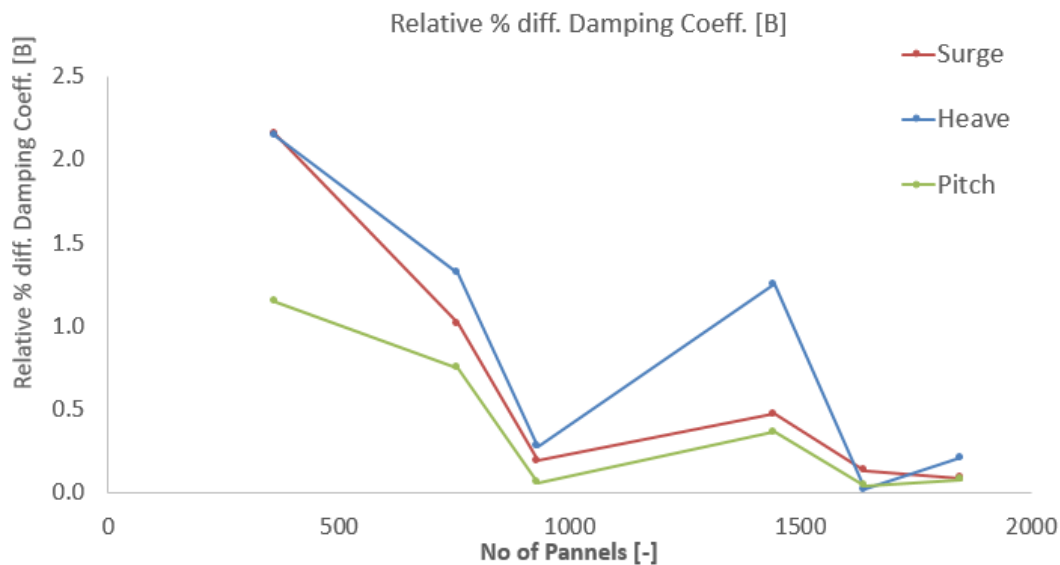
Figure 14: Rel.% diff Damping Coeff. in NEMOH

In the Fig. 14,the relative percentage difference for damping coefficient are plotted. From the figure, it shown that in surge for initial panel size of 361, it was 2.14 % and and it was reduced for panel size of 930. But it shown a bit abnormality similar to diffraction force amplitude and added mass coefficient and increased for panel size of 1443 and then it decreased to 0.088 % for panel size of 1848.

In the heave motion of cylinder, the relative % difference in damping coefficient was 2.14 % for initial panel size of 361, then it reduced for panel size of 930 similar to surge but very slight huge increase was seen for panel size of 1443. It then reduced back for panel size of 1638 and it further increased to 0.214 % for panel size of 1848. Whereas for pitch motion, it shown similar behaviour as surge.

4.2.1   Conclusion

From the convergence analysis of forces, added mass and damping coefficients, it can be concluded that there is a considerable decrease in the parameter values from panel size of 361 to 930 in all the cases and dofs. But after simulation with panel size of more than 930, relative % difference in Froude-Krylov seems to have non-considerable difference. Diffraction forces fluctuated at panel size of 1443 as mentioned before but again it reduced to panel size at 1638 and so on panel size at 1848 and same behaviour shown by the added mass and damping

coefficient.

Although the relative percentage difference of the forces and the coefficient seem to have a small at max panel size at 1848 but the computational time required at this panel size was huge compared to panel size of 1638. Even percentage difference at later panel size seen to be converged close to zero except few parameters. But finally a trade off between the converged value and computational time done and panel size of 1638 (target panel size 1800) was taken as converged panel size.

Note that post convergence analysis for WS and NEMOH, a converged mesh sizes ($dx1$, $dx2$ and $dx3$) and similarly a converged panel number for NEMOH were obtained. This converged sizes are used for all the simulation in later parts of this thesis.

Table 4: Converged mesh/panel sizes

Solver	Converged mesh/panel size		
Weak-scatterer	x1 = 0.75	x2 = 0.05	x3 = 0.05
NEMOH	1638		

In the Fig. 15 and 16 below, the converged panel and mesh sizes for NEMOH and WS shown respectively. Whereas for NEMOH, the converged panel size was considered around 1800 and for weak-scatterer code, the converged mesh sizes were $dx1 = 0.75m$ and $dx2 = dx3 = 0.05m$ as tabulated in the Table 4.
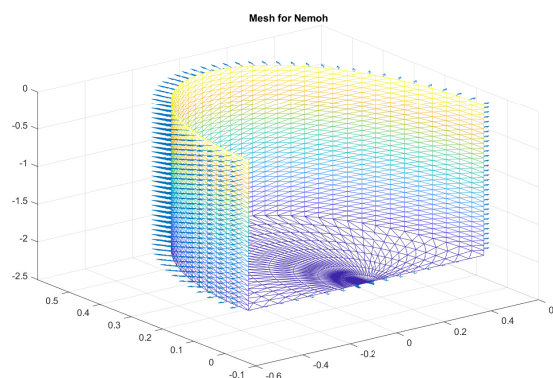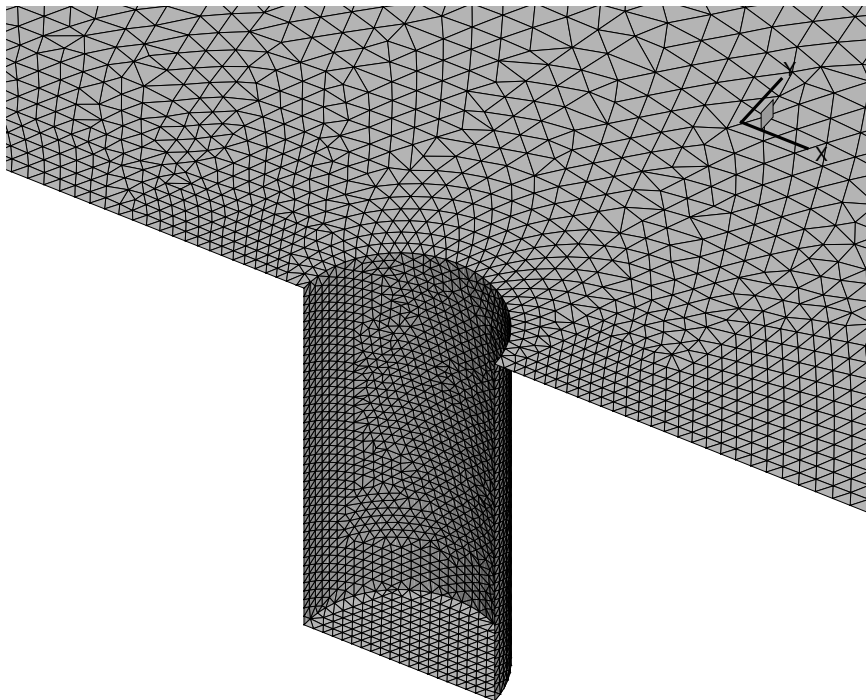

Figure 15: converged panel for NEMOH

Figure 16: Converged mesh sizes for ws

4.3   Low Steepness

4.3.1   Fixed Body

4.3.1.1   Linearised Free Surface and Body

As mentioned in the heading, in this case a small steepness case with Fixed Body (means all the DoFs in the input file are given as False), Linearised Free Surface and Body Motion (means Linearised Free Surface and Body Motion in the input file are given as True) are taken into consideration. So, this case was totally a linear sea-keeping test case and comparison of the outputs of this case with linear code NEMOH could be highly appreciable. The wave parameters which are taken as follows:

Parameters	Value
Pulsation (rad/s)	3.74
Amplitude (m)	0.01
Wavelength (m)	4.41
Steepness	0.045
Direction (rad)	0
Phase (rad)	0

Table 5: Input wave parameters

With above wave input parameters as mentioned in the above table 5 , the simulation was performed for the cylinder. Post simulations, the result are plotted as follows:
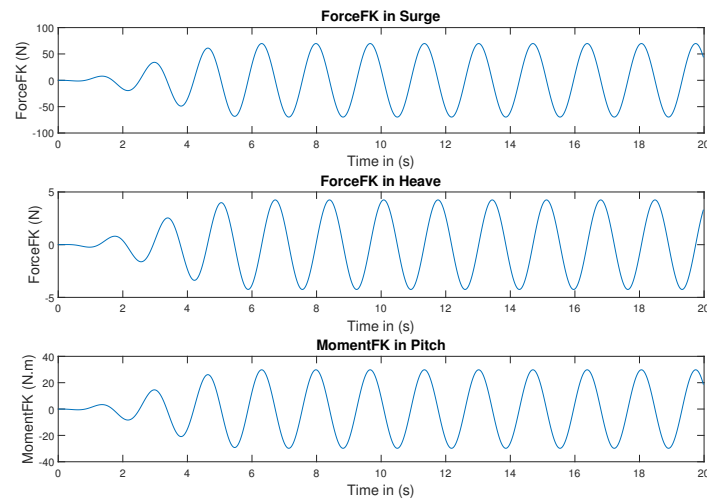
Figure 17: Force (Froude-Krylov) for fixed body fully linear case for steep 0.45 %
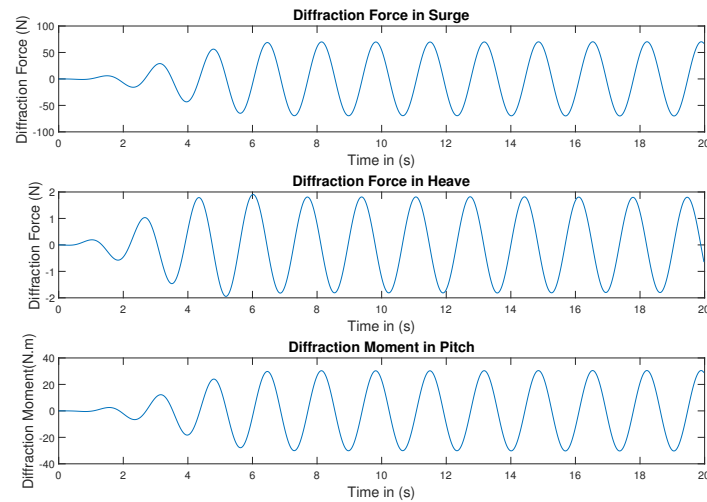

Figure 18: Diffraction Force for fixed body fully linear case for steep 0.45 %

It can be seen in Fig. 17, the Froude-Krylov forces exerted on the cylinder are plotted in the time domain. Similarly, in the Fig. 18 the diffraction forces are plotted. These forces are periodic in nature and initial deviation for periodicity exist due to ramp-up period are taken till 6 s.

Then, these forces obtained in the WS were compared with linear code NEMOH to understand non-linearities if exist.

4.3.1.2 Comparison with NEMOH

In this section, the comparison of the forces exerted on cylinder were drawn with NEMOH to validate the result obtained from WS with linearised assumption (fixed body, linearised FS and linearised body). To draw the comparison between then, the incident forces (Froude-Krylov) and diffraction forces were compared between them. Note that since body being fixed there are no chances of radiation forces so it becomes null obviously and was not taken into account. Since, due to nature of NEMOH being in Frequency domain, the amplitude of the these forces were converted to time domain.
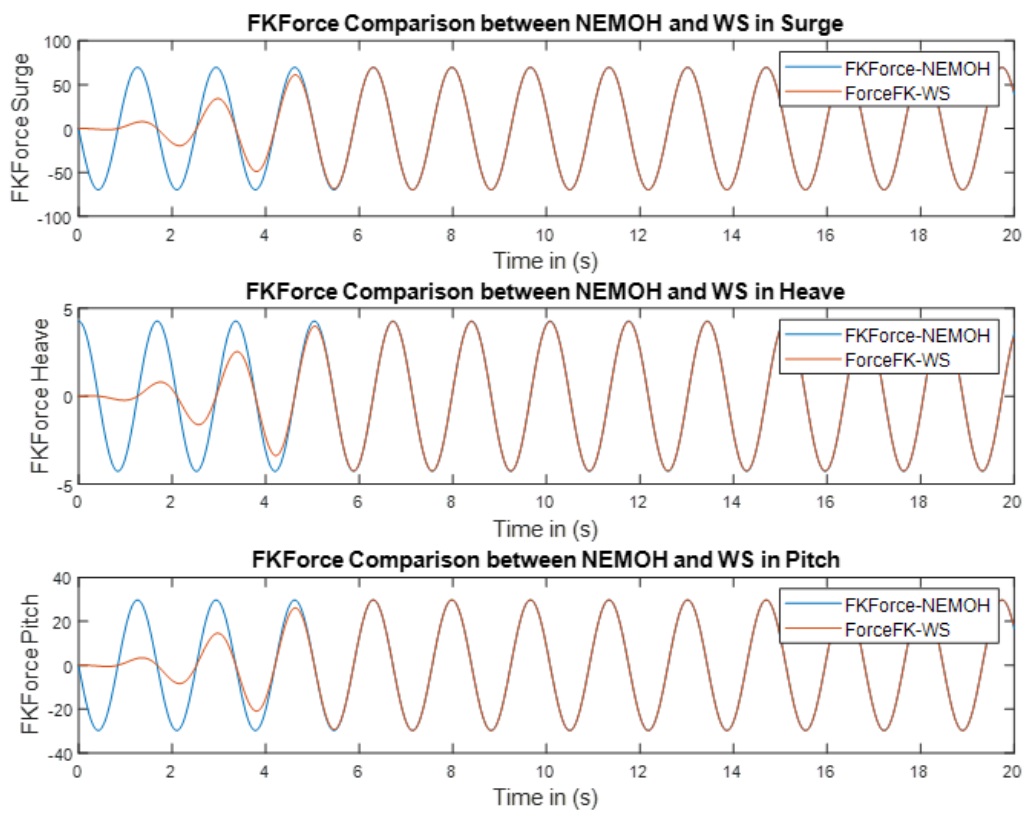

Figure 19: Comparison of Forces (Froude-Krylov) for converged mesh between WS and NEMOH
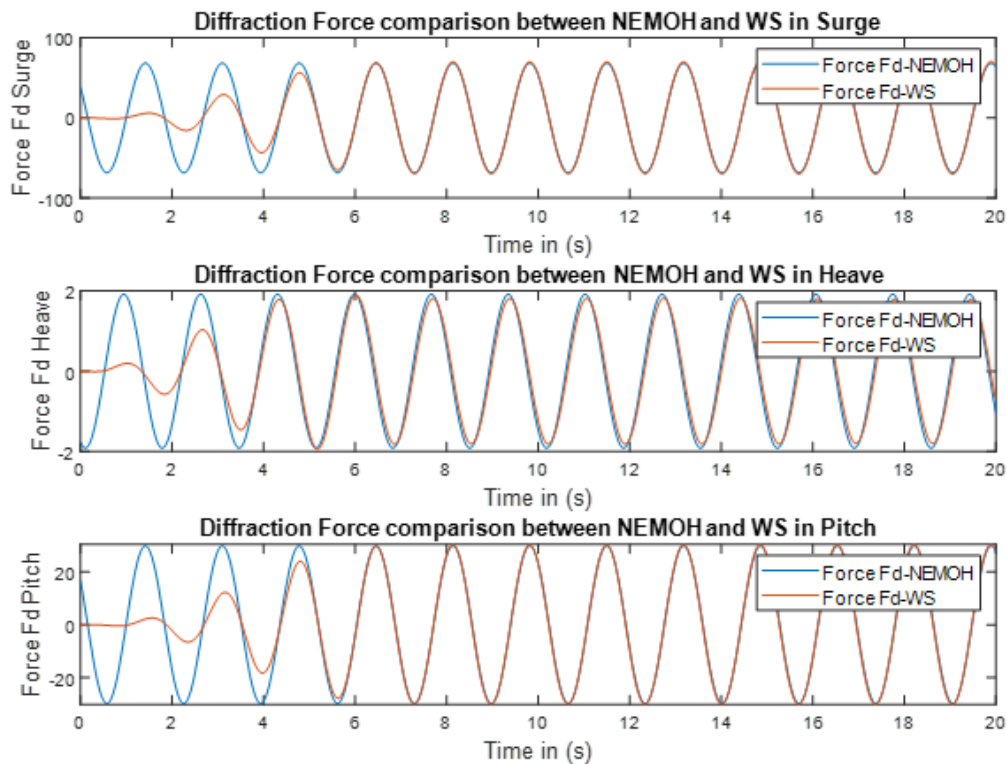
Figure 20: Comparison of Diffraction Forces for converged mesh between WS and NEMOH

From above comparison following comparison can be drawn:

- From Fig. 19, it can be seen that Froude-Krylov forces were quite similar in both the case and superimpose each other. Only difference can be seen till 6s which was due to time instant for initial ramp was taken upto 6s.

- Whereas, in the Fig. 20, again it can be seen that Diffraction forces too were quite similar in linearised Weak-scatterer and NEMOH in Surge and Pitch. The discrepancy can be seen in heave case, where although the amplitude of the diffraction forces were quite same in both case but phase difference can be seen, which is quite unexpected. This could be possibly due to convergence or also presence of the quadratic term in pressure.

4.3.1.3 Non-linear Free Surface and Body

In this section, the study was performed for sea-keeping test case through addition of the numerical non-linearities. As explained in the previous section

that addition of the numerical non-linearities means inclusion of non-linear free surface and body non-linearities. This is the first interesting test case of this Master thesis from objective of the thesis point of view. As the previous case of linearised weak-scatterer case non-linearities was absent.

Post inclusion of the non-linear free surface and body non-linearities in the input file of the simulation, the simulation was performed and forces exerted on the vertical cylinder was quantified.

To estimate the numerical non-linearities, the forces exerted on the vertical cylinder were compared with the previous test case i.e. linearised weak-scatterer test case, which is evident from the Fig. 21 and Fig. 22.
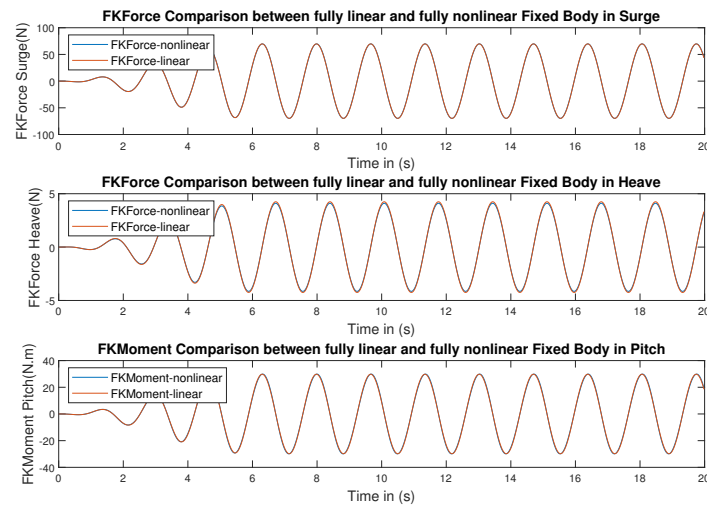

Figure 21: Comparison of Forces (Froude-Krylov) for converged mesh between fully linear and fully non-linear
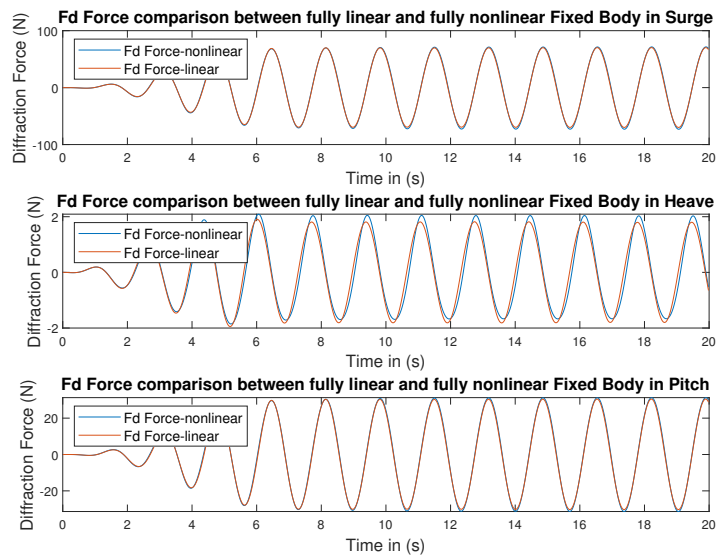
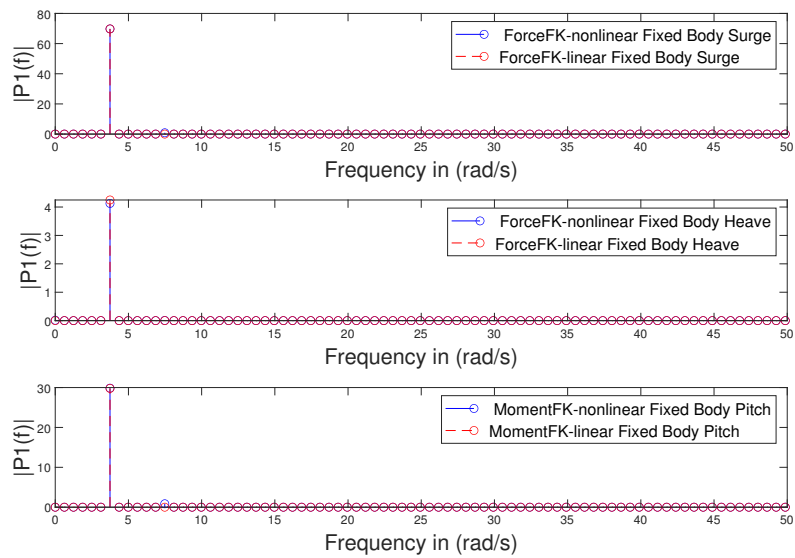**Figure 22:** Comparison of Diffraction Forces for converged mesh between fully linear and fully non-linear

Figure 23: FFT of Comparison of Forces (Froude-Krylov) for converged mesh between fully linear and fully non-linear
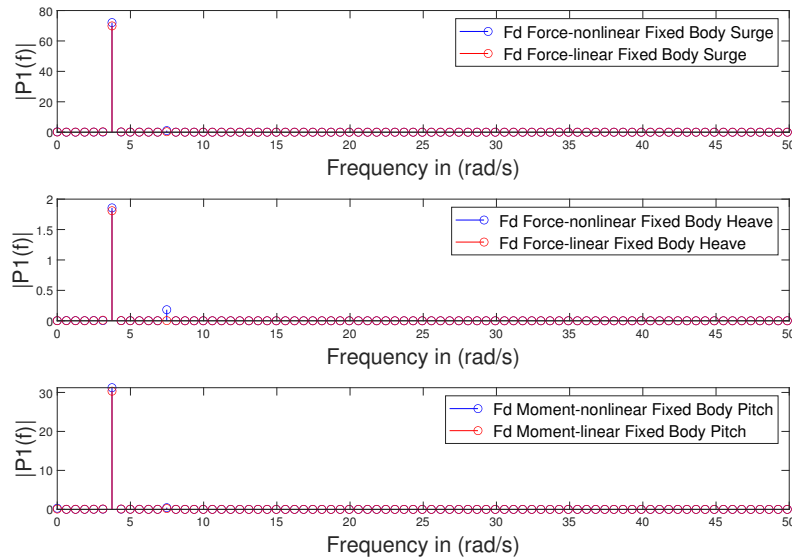
Figure 24: FFT of Comparison of Diffraction Forces for converged mesh between fully linear and fully non-linear

From the Fig. 21 , the comparison of the Froude-Krylov forces in this test case with previous showed an interesting results. Although there exist an inclusion of numerical non-linearities (non-linear free surface and body) in the simulation but the forces didn't exhibit any non-linear behaviour. So phase and amplitude of the Froude-Krylov forces in both non-linear and linear remain same here because this test case is physically linear.

On the Fig. 22 show the comparison of the diffraction forces. It can be seen that in Surge and pitch, there exist no non-linearities but small non-linearities can be seen in the case of heave.

To understand the presence of the noisy disturbances in the signal, frequency domain are more preferred than time domain since it is easy to identify through frequency domain. On the same analogy, the FFT plot of the comparison of forces were plotted so that any non-linearity present will be visible.

From the Fig. 22, it can seen that FFT were plotted for the comparison of the Froude-Krylov forces in the case of non-linear and linear case for steepness of 0.45%. But, absence of the non-linearities was seen in the Fig. 21 so FFT plot also exhibit similar behaviour.

On the other side, FFT were plotted for comparison of the diffraction forces in Fig. 24, here it can be seen that in the Surge and Pitch, the amplitude of the

power are same at first harmonic but small non-linearities were visible in the heave case at first harmonic and very small amplitude at second harmonic.

4.3.2 Free Body

4.3.2.1 Linearised Free Surface only

In the last section, it was found that Weak-Scatterer test case with Small Steepness of 0.45%, fixed Body, linearised free surface and body motion are totally linear in nature. The forces exerted on the vertical cylinder in this test case perfectly resemble with linear code NEMOH.

On the other hand, the test case with non-linear free surface and body with fixed body, exhibited very minute non-linearities in diffraction forces in heave. As the objective lies in the determination of non-linearities, so we need to move from partially non-linear (non-linear free surface body with fixed body) to non-linear (non-linear free surface body with free body), for that 3 degree of Body were freed.

It should be worth mentioning here that WS code presently not working well with free body (only surge, heave & pitch) with Linearised Free Surface only. The reason could be as follows:

- WS with Free Body work along with movement of meshes of the free-surface, and if meshes of the body are moving and meshes of the free-surface are fixed. It creates un-stability of the simulation and it crashes.

- There could be another reason of stability of the weight and buoyancy of the body, but simulations were also performed with lower centre of gravity of body to create enough metacentric height but still simulation crashes.

- Other efforts were made by either linearising the body meshes but FS being non-linear or vice-versa but situations remains unchanged.

- From above simulations, a lesson was learnt that if body is free which is non-linear in nature due to its movement, the free surface and body should be non-linearised to stabilise the simulation and avoid errors.

4.3.2.2 Linearised Free Surface and Body

This test case is not relevant to study because linearising the free surface and body both in the case of the free body motion doesn't make sense at all. The reasons behind this argument are following:

- When we linearise the free surface, the meshes of the free surface get fixed. Then while linearising the body, the meshes get still. Now this test case being free body case with fixed mesh of free surface and body, it can destabilise the simulation and crashes or can give invalid results.

To support this argument , the simulation was performed to tests case of Free Body, Linearised Free Surface and Body both and the results were plotted below:
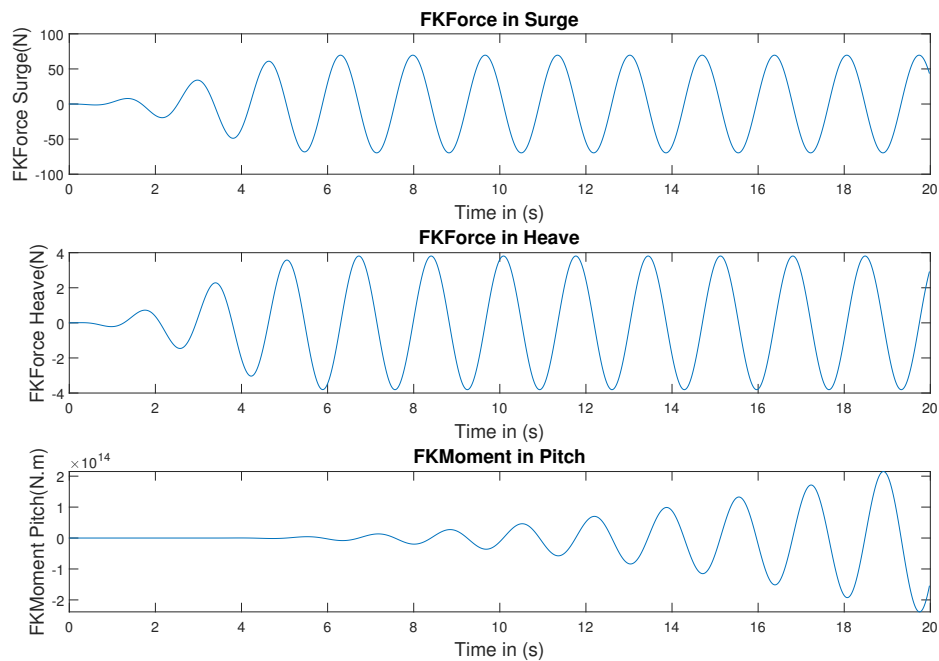

Figure 25: Force (Froude-Krylov) for free body fully linear case for steep 0.45 %
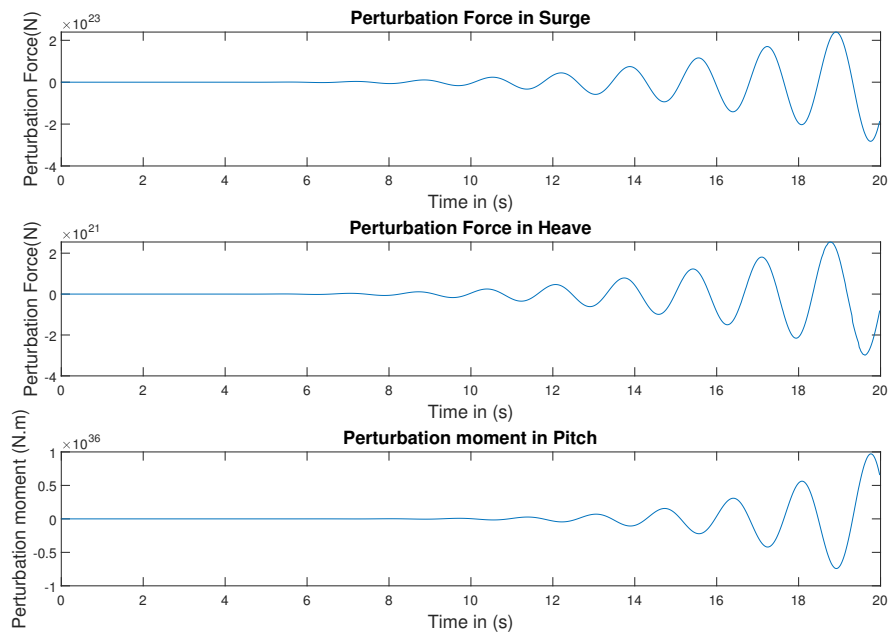
Figure 26: Perturbation Force for free body fully linear case for steep 0.45 %

As initially argued, linearised free surface and body in the case of free body doesn't make sense at all for the aforementioned reasons . So post simulation, plotting the forces in the time domain it is seems that it is quite huge in nature and far from reality. Through learning lesson with this test case, this test case were avoided later while changing the physical non-linearity(steepness).

4.3.2.3 Non-linear Free Surface and Body

After lesson learnt from the previous test case, the free surface and Body was non-linearised in the input file and simulation was performed with converged mesh sizes in weak-scatterer. Post simulation, the Froude-Krylov and diffraction forces areplotted in the time domain in the Fig. 27 and 28.
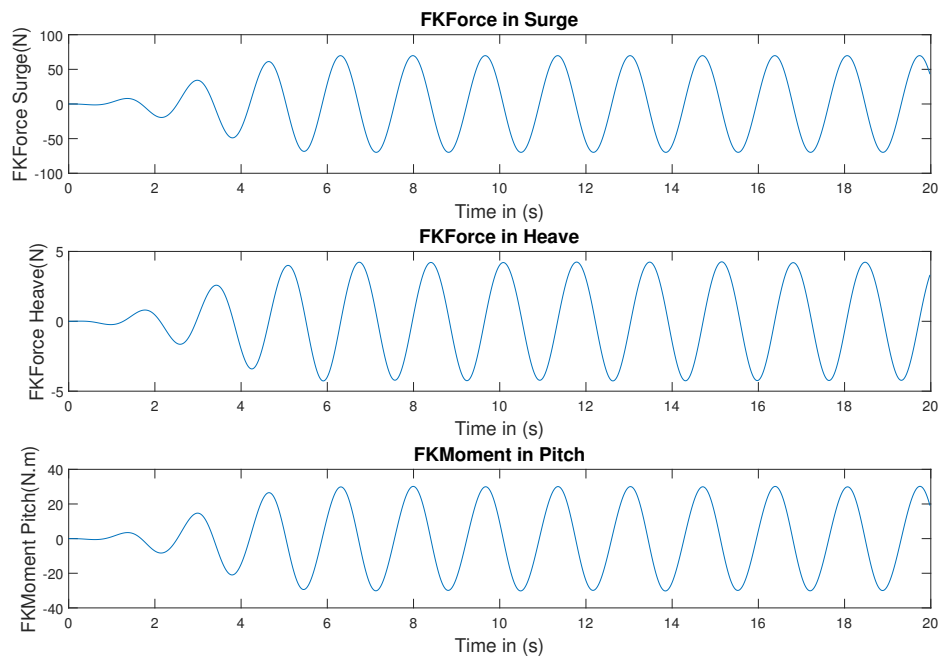
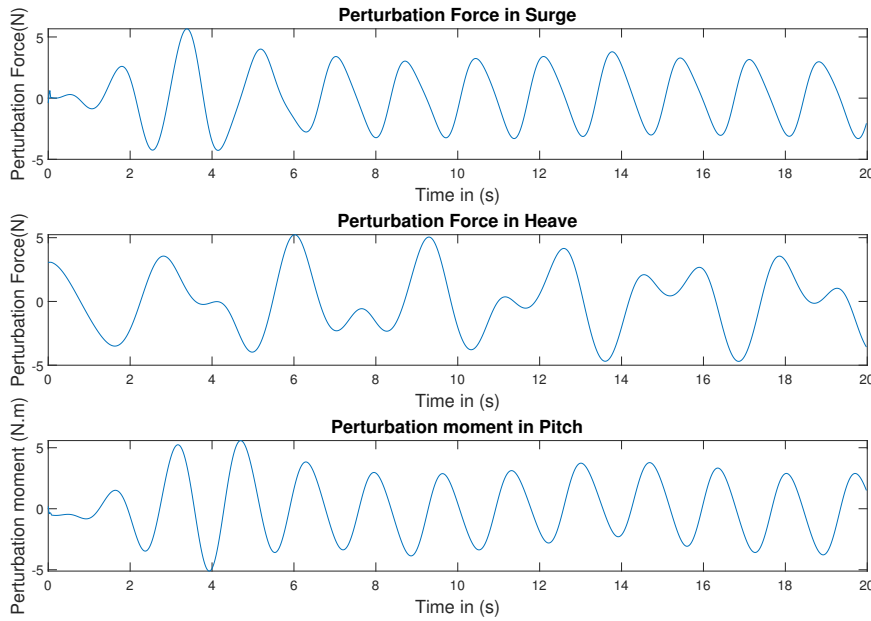**Figure 27:** Force (Froude-Krylov) for free body fully non-linear case for steep 0.45 %

Figure 28: Perturbation Force for free body fully non-linear case for steep 0.45 %

From Fig. 27, it can be seen that Froude-Krylov forces were still periodic in nature and still non-linearity is absence.

On the other hand, Fig. 28 shown that good amount of non-linearities present in the test case for the calculation of pertubation forces. Although the plot of perturbation forces in surge and pitch follow a bit periodic nature but in heave, the non-linearities were quite visible.

Next, the forces (Froude-Krylov and Perturbation) exerted on the vertical cylinder were compared with NEMOH. As NEMOH doesn't give the perturbation forces directly from its solver. So, a code was written to calculate the Radiation forces from the NEMOH with the help of added mass and damping coefficient and then added with diffraction forces to get the total perturbation forces.

$$F_R = \sum_{j=1}^{6} \mu_{ij} \ddot{X}_j(t) - \sum_{j=1}^{6} \lambda_{ij} \dot{X}_j(t) \tag{29}$$

Where μ_{ij} and λ_{ij} are known as the added mass and damping matrix respectively.

Now taking into account for

$$X(t) = Re(Xe^{-i\omega t}) \tag{30}$$

Equation 29 can be written as:

$$F_R = [-\omega^2 \mu_{ij} - i\omega\lambda]X \tag{31}$$

In the others words, the Equation 31 can be written as :

$$F_R = [-\omega^2 A(\omega) - i\omega B(\omega)]X(\omega) \tag{32}$$

Where, A and B are known as the added mass and damping matrix respectively taken from the NEMOH simulation.

Now, the total perturbation forces are calculated as follows:

$$F_P = F_D + F_R \tag{33}$$

Where, F_D are the diffraction forces calculated from NEMOH and F_R are the radiation forces calculated from equation 32.

Then, these Froude-Krylov and perturbation forces in both the test case were compared in Fig. 29 and Fig. 30.
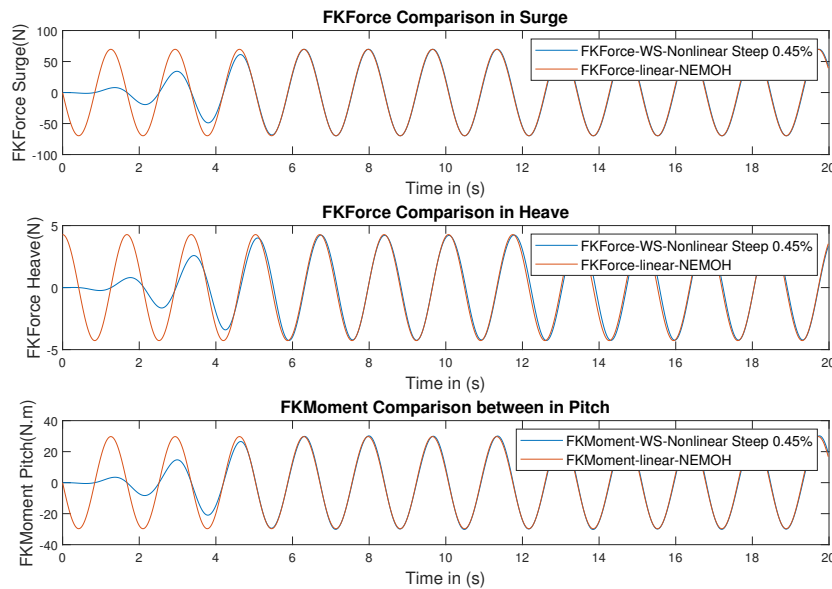

Figure 29: Comparison of Forces (Froude-Krylov) for converged mesh between fully non-linear WS and NEMOH
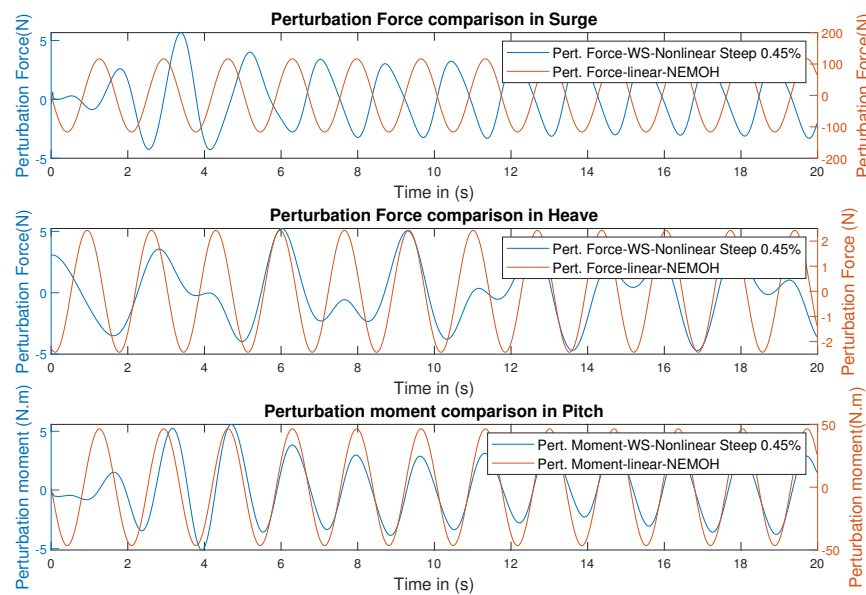
Figure 30: Comparison of Diffraction Forces for converged mesh between fully non-linear WS and NEMOH

It can be seen from the Fig. 29, the Froude-Krylov forces are compared and found to in very good agrement except in the ramped up zone of 6s. Whereas in Fig. 30, the perturbation forces are compared and results are found to be paradigm shift from the previous plot. Here, following observations can be made:

- The first and the foremost observation can be found that the order of the magnitude of perturbation forces. In the case of nonlinear free surface and body with free body test case, perturbation forces found to be 30 times lesser in surge, 10 times lesser in pitch and around same in heave.

- The perturbation forces plot in Fig. 30, shows a small periodicity in surge and pith but in heave periodicity were vanished which shows huge presence of non-linearity.

Investigation were also made to find out the possible reason foor the drastic change in the perturbation forces in this case compare to linear one fixed body test case in NEMOH. It was found in free body of this case, vertical cylinder move in opposite direction of the wave propagation so incoming waves counteract the perturbation forces exerted on the body in the different phase and it finally

cancel it out a huge quantity of the perturbation forces. That could be the possible reason of the drastic reduction in the free body case of with non-linear free surface and body.
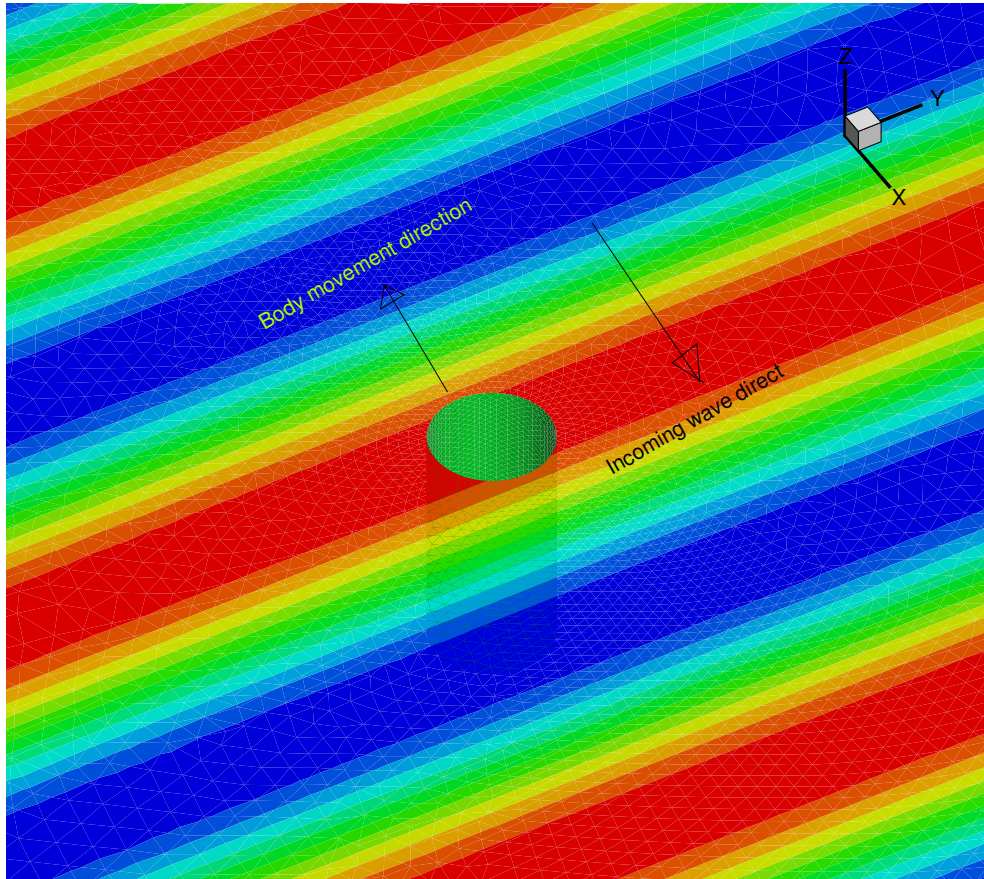

Figure 31: Counteract motion of cylinder

4.4 High Steepness

In this section, the steepness of wave was increased to 0.45% to 5%, i.e. the amplitude of the wave was increased to $0.11m$ from $0.01m$ while keeping all the parameters same. Since the main objective of this section to understand the linearities originated due to change in the physical non-linearity (wave steepness).

4.4.1 Fixed Body

4.4.1.1 Linearised Free Surface and Body

As usual, the first computation was performed with less complex test case of cylinder being fixed (i.e. degree of the freedoms of the motion of cylinder were restricted) and both free surface and body were linearised as well. Body being stationary and linearisation of Free surface and body, the first simulation with change in physical non-linearity was performed. The forces obtained in this test case are plotted below in Fig. 32 and 33.
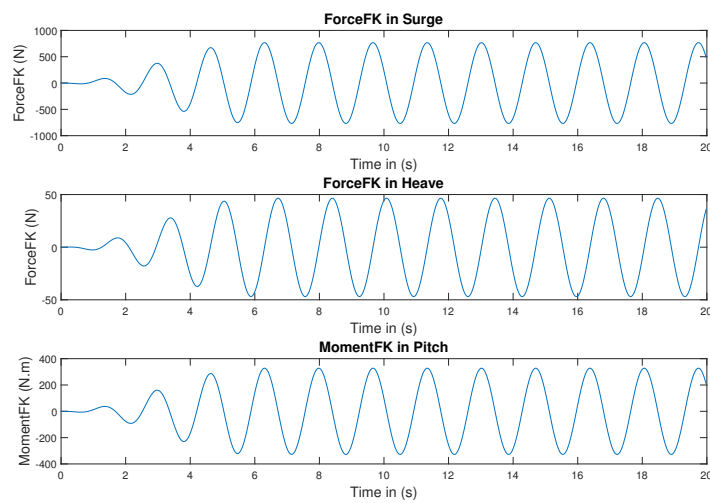

Figure 32: Forces (Froude-Krylov) for converged mesh for steepness 5 percent
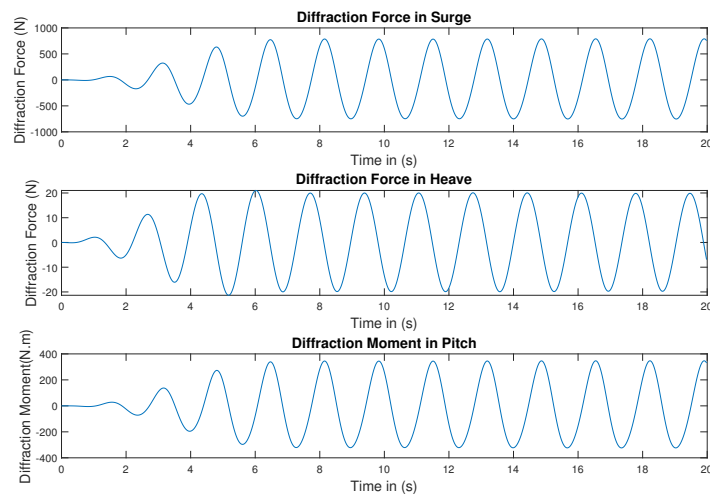
Figure 33: Diffraction Forces for converged mesh for steepness 5 percent

From the above two figures, it can be seen that the Froude-Krylov forces for wave of steepness 5% are increased upto order of 10 compared to Froude-Krylov forces for wave of steepness 0.45%. Similar increase can be seen in the case of diffraction forces.

So, to compare these forces of different order of magnitude to understand the non-linearity due to changes in physical non-linearity through the steepness of the wave, these forces (Froude-Krylov and diffraction forces) need to normalised with respect to wave amplitude so that comparison could be more reasonable.

Hence, these forces of steepness 5% are normalised with respect to steepness and compared with normalised forces of steepness 0.45% in the following figures.
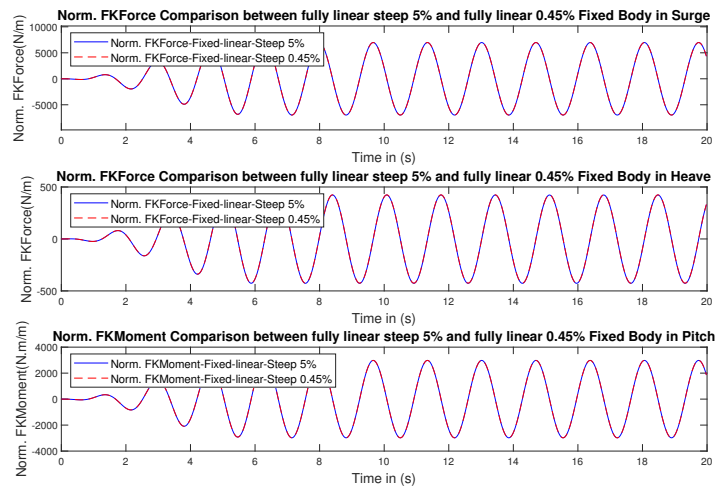
Figure 34: Comparison of Norm. Forces (Froude-Krylov) for converged mesh between fully linear steep 5% and fully linear steep 0.45%
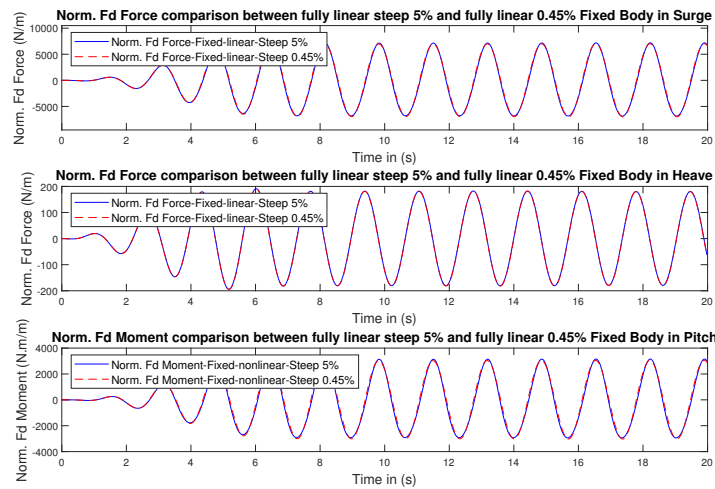

Figure 35: Comparison of Norm. Diffraction Forces for converged mesh between fully linear linear steep 5% and fully linear steep 0.45%

From the Fig. 34 and 35, it can be seen that the differences between Froude-Krylov forces and Diffraction forces are about negligible. To better appreciate the linearities if any present, the FFT plots were plotted for these normalised forces. From these FFT plot for Froude-Krylov forces and Diffraction forces in

Fig. 36 and 37, again it can be seen that no non-linearities present for Froude-Krylov forces but very small amount can be seen for diffraction force. Hence, the non-linearity associated between test cases of fully linear fixed body in steepness of 0.45% and 5% was presnet in the very small amount in Diffraction forces.
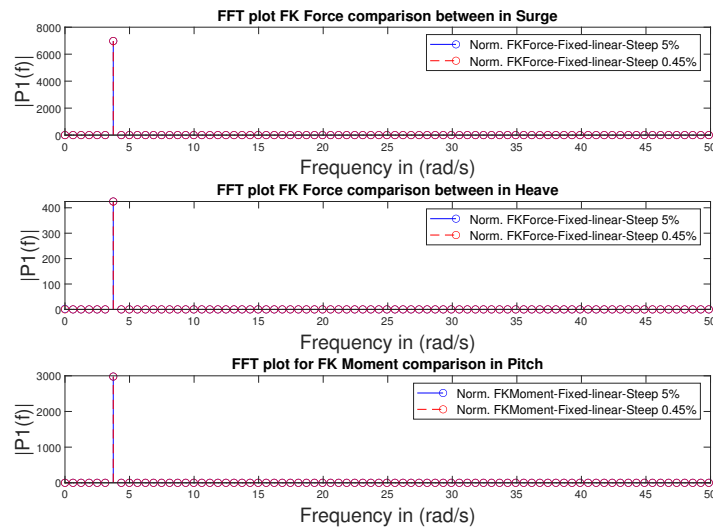

Figure 36: FFT of Comparison of Norm. Forces (Froude-Krylov) for converged mesh between fully linear steep 5% and fully linear steep 0.45%
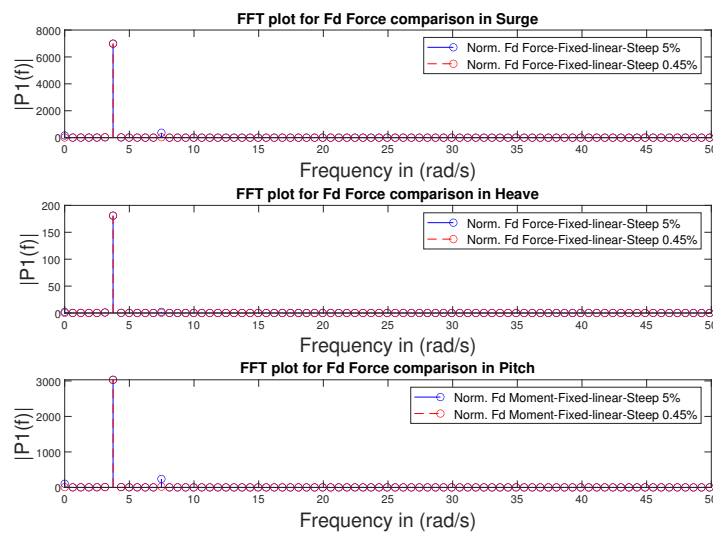
Figure 37: FFT of Comparison of Diffraction Forces for converged mesh between fully linear and fully non-linear

4.4.1.2 Non-linear Free Surface and Body

The test case of fully linear fixed case of wave steepness 5% shown that absence of non-linearities in forces although there remain a physical change of non-linearities due to changes of steepness from 0.45%. The main reason for the absence of the could be omission of numerical non-linearities such as Free surface and body.

This test case was considered while taking into account of the both numerical non-linearities such as Free surface and body as well as physical non-linearity such as change in steepness from 0.45% to 5%.

Again the forces are normalised with respect to steepness of 5% and compared with test case of fully non-linear normalised forces of steepness 0.45% in the figures below.
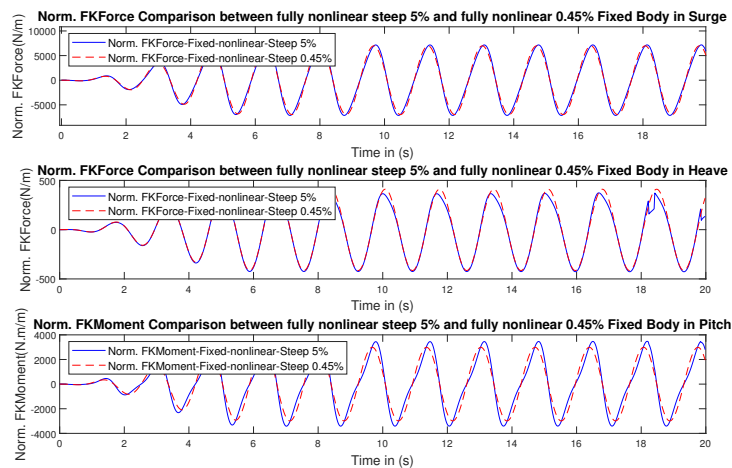
Figure 38: Comparison of Norm. Forces (Froude-Krylov) for converged mesh between fully nonlinear steep 5% and fully nonlinear steep 0.45%
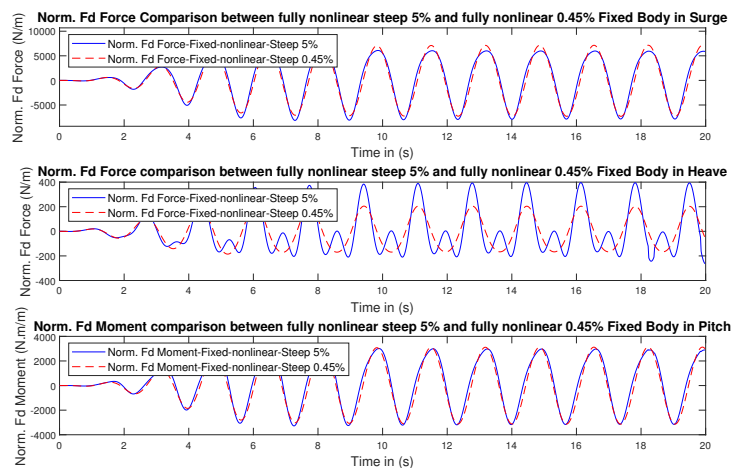

Figure 39: Comparison of Norm. Diffraction Forces for converged mesh between fully nonlinear steep 5% and fully nonlinear steep 0.45%

From Fig. 38, it can be seen that the Froude-Krylov forces in Surge exhibit a little differences. Whereas in Heave and Pitch, the differences is quite huge. Similary from Fig. 39, it seems that diffraction forces for fully non-linear test case of steepness 5% are more exhibit-able compared to Froude-Krylov forces in Surge. In the Heave, differences are quite huge and the non-linear nature of plot

of forces can also been seen as compared to diffraction forces for fully non-linear test case of steepness 0.45% in Fig. 35 .

To show the non-linearity better, FFT are plotted for the normalised forces for above non-linear test cases below:
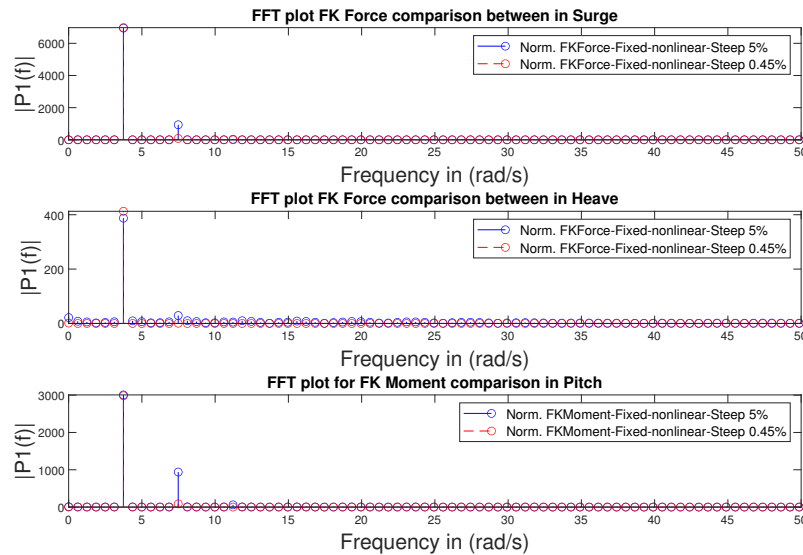

Figure 40: FFT of Comparison of Norm. Forces (Froude-Krylov) for converged mesh between fully nonlinear steep 5% and fully nonlinear steep 0.45%

From the FFT plot in the Fig. 40, it can be seen that as expected in the Surge case, the amplitude of the normalised forces are same at first harmonic frequency but due to presence of non-linearity another amplitude is present at the 2nd harmonic frequency. In the case of Heave, as exist a difference in the amplitude in both the test cases, so at first harmonic, the amplitude is quite same but small amplitude can be also seen at the 2nd harmonic. Some non-linearities can also be seen in the form of small disturbances in signal around x-axis in blue circles.

Similarly in the case Pitch of Fig. 40, it can be seen that signal are same at first harmonic but at the 2nd harmonic, the amplitude of the signal has increased as compared to Heave case but other small disturbance signal around x-axis is very rare.
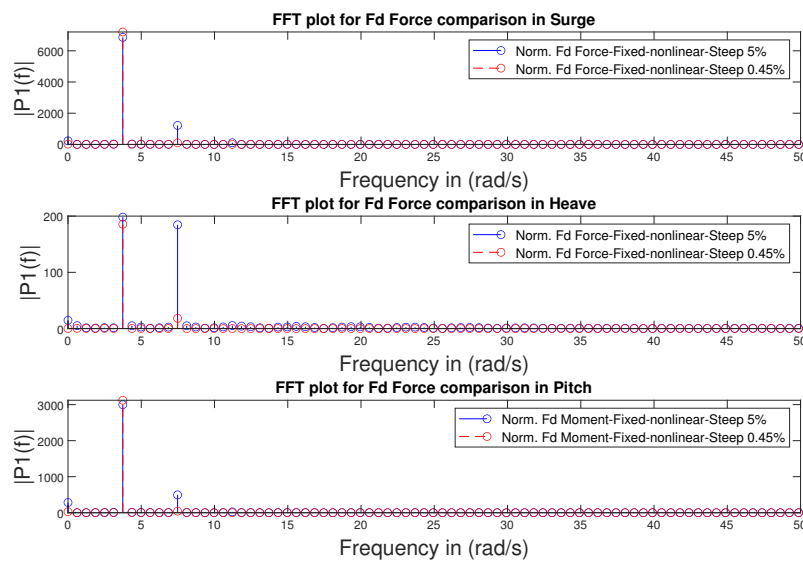
Figure 41: FFT of Comparison of Diffraction Forces for converged mesh between fully nonlinear and fully nonlinear

From the Fig. 41, it can be seen that for Surge case, amplitude of the signal at first harmonic is same but as evident from comparison the differences due to physical non-linearity (increase in steepness)has led to 2nd harmonic signal. In the case of heave, as the differences are more prominent so at first harmonic behaviour are same as heave but at 2nd harmonic, the amplitude of signal quite high as compared to previous. Whereas in the case of Pitch, the behaviour is as similar to heave.

4.4.2 Free Body

4.4.2.1 Non-linear Free Surface and Body

In this case, a test case was set-up with non-linear free surface and body for same steepness. This test was run for various mesh size including the converged and coarsest mesh. But it was found that the test case doesn't run successfully for these mesh size. As the moderate mesh sizes run successfully for some of the test case in free body for steepness of 0.45 %, so trials were made with these moderate mesh sizes, nevertheless test case didn't succeed.

While investigating the reason, it found that first body meshes around free surface start distorting at about 11.84 s as shown in Fig. 42 and then it extend

other part of the body gradually as shown in Fig. 43. Then, the body meshes distort upto such extent that it destabilise and crashes the simulation.
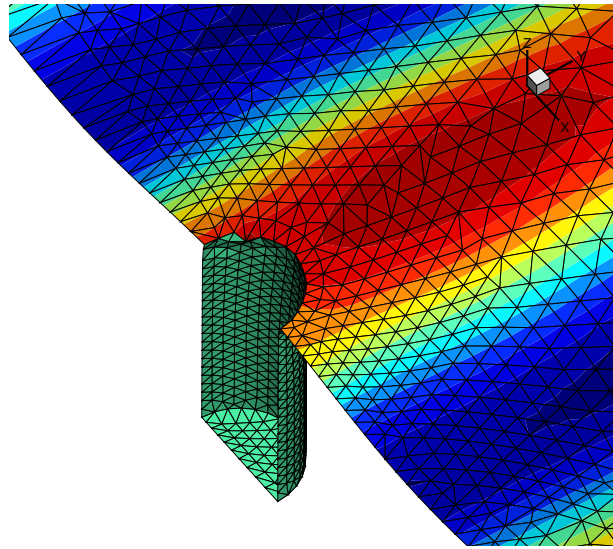

Figure 42: Body mesh distortion around free surface at 11.84 s
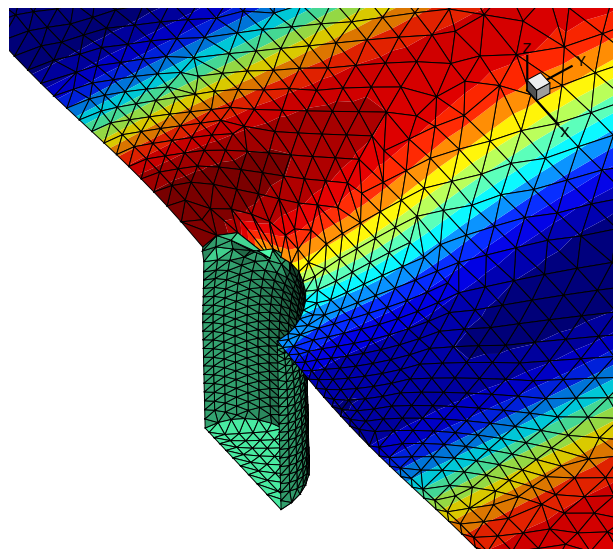

Figure 43: :Body mesh distortion at 13.16 s

From the above two figure, it was explained that the simulation crashes after 13s. Although forces are plotted in the figures below to understand their behaviour.

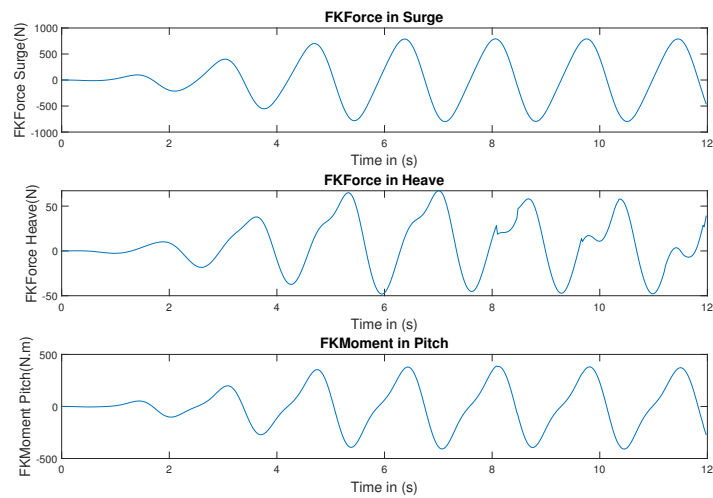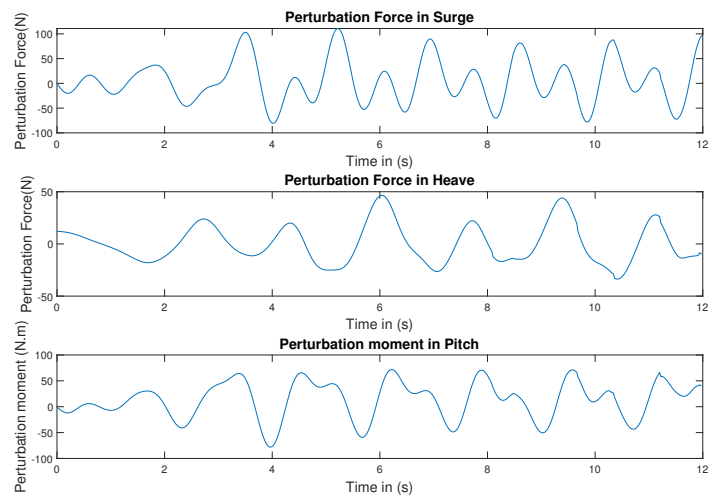**Figure 44:** Forces (Froude-Krylov) for free body fully nonlinear for steepness 5 percent

Figure 45: Perturbation Forces for free body fully nonlinear for steepness 5 percent

In the Fig. 44 and 45 it can be seen that forces were plotted in the time domain plot till 12s only since as mentioned before simulation crushed at 13s. From both plots it can be seen that good amount of non-linearities present in the both the forces.

As this case belong to higher steepness with free body non-linear test cases, so it was interesting to compare the normalised forces exerted on the cylinder to the lower steepness with free body non-linear test case. These comparison were plotted in the Fig. 44 and 45. From these plot it is evident that increase in the steepness (physical non-linearity) caused a good amount of non-linearities which was expected.
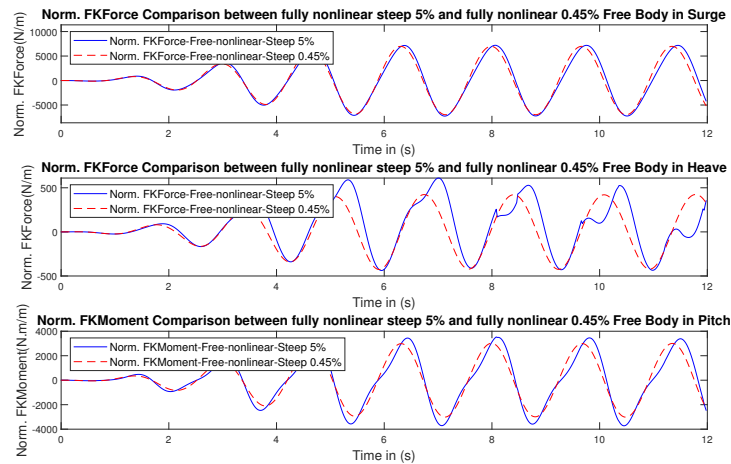
Figure 46: Comparison of Norm. Forces (Froude-Krylov) for free body fully nonlinear steep 5% and fully nonlinear steep 0.45%
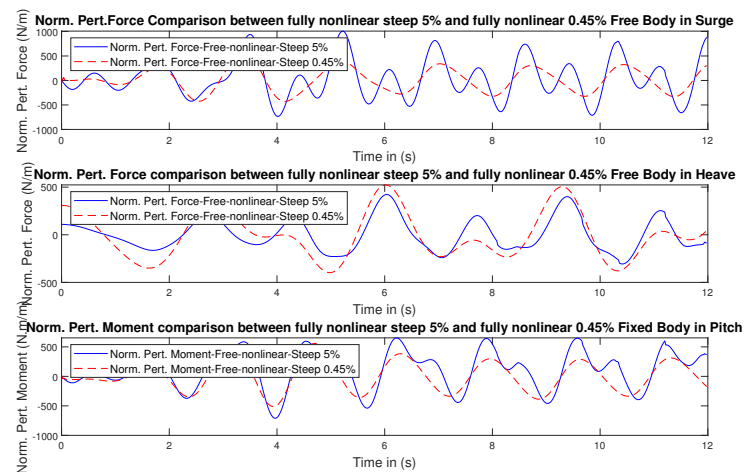
Figure 47: Comparison of Norm. Perturbation Forces for free body between fully nonlinear steep 5% and fully nonlinear steep 0.45%

5   Conclusions

In this Master thesis, study of the seakeeping non-linearities through the weak-scatterer approximation of the potential flow theory was performed. This study was undertaken on a vertical cylinder and the forces acting on this cylinder was taken into account to evaluate the non-linearities.

An overview of the literature was done to understand the different potential flow solver and place of weak-scatterer solver among these solvers. It was found that linear solver are quick and computationally affordable whereas fully non-linear solver are highly computationally expensive. The weak-scatterer non-linear are placed under middle ground which is both quick, computationally affordable and almost accurate. Under this, the past studies about this approach and recent advancements at LHEEA were also studied.

The study was undertaken through simulation of weak-scatterer code with aforementioned vertical cylinder. In the first simulation, the code was simplified through inputs of linearised free surface and body. After the valid result of the first simulation, convergence study was performed with a numbers of mesh size and finally a converged mesh size was found for weak-scatterer.

The first simulation/test case was performed with inclusion of linearised free surface and body inputs with fixed body to the Weak-scatterer code, so comparison of the forces with linear code NEMOH code would be interesting. From that view, simulation of the vertical cylinder was performed in NEMOH but before comparing the result, convergence study was performed in NEMOH too to get the mesh-independent result. Then, the result from both the methods were compared and found to have comparable results.

The main objective of the thesis was to study the non-linearities associated with weak-scatterer approach. So, in next test case keeping numerical non-linearities were included through inclusion of non-linear free surface and body while keeping all the other parameter same. After simulation, this test case result was compared with previous WS linear test case. It was found that in the Froude-Krylov forces non-linearities were absent but small presence was seen in the diffraction forces.

In the next test case, another numerical non-linearities were added in the form of free body and simulation were performed for linearised free surface only and found that it was not worked properly and lessons were learnt for future test cases that linearised free surface with free body lead to possible instability of mesh. Therefore, in the continuation of the previous test case next test case was performed with non-linear free surface and body . The forces (Froude-Krylov and perturbation)exerted on the cylinder were compared with NEMOH's result

and found the it showed good amount of non-linearity but perturbation forces also reduced drastically. The hypothesis were put that possible reason could be counteracting motion of the cylinder in the line with incident wave direction.

Previous test cases were performed with the inclusion of the numerical non-linearities but next test case was with inclusion of the physical non-linearity means changing from small steepness (0.45%) to higher steepness (5%) while keeping the weak-scatterer code to linear and cylinder to be fixed. While comparison with previous low steepness case, it was found that non-linearities in totally absent in this test case. In the next case, while keeping cylinder to be fixed and inclusion the physical non-linearities and numerical non-linearities (non-linear free surface and body), sea-keeping test case was performed. A good amount of non-linearities was found to be present in the forces. Next test case was performed with keeping all the previous parameters with addition of free body, found the simulation crashes.

Therefore, from the various test cases were performed and good amount of the non-linearities was found in the test case of free body with non-linear free surface and body with steepness of 0.45% and fixed body with non-linear free surface and body with steepness of 5%. The test case of free body with non-linear free surface and body with steepness of 5% would be interesting to discuss but as aforementioned the simulation crashes.

The future perspectives of this master thesis can following:

- The entire test cases in this master thesis were run without forward speed. It would be interesting to couple the forward speed in the simulation.

- The mentioned before, the test case of free body with non-linear free surface and body with steepness of 5% would be interesting to discuss but the simulation crashes.

- This master thesis can be also extended to non-academic geometry.

Bibliography

[1]   URL: https://en.wikipedia.org/wiki/Helmholtz_decomposition.

[2]   URL: http://www.principia-group.com/blog/product/diodore/.

[3]   URL: https://marine-offshore.bureauveritas.com/hydrostar-software-powerful-hydrodynamic.

[4]   URL: https://lheea.ec-nantes.fr/valorisation/logiciels-et-brevets/nemoh-presentation.

[5]   URL: https://www.wamit.com/.

[6]   URL: https://www.ansys.com/fr-fr/products/structures/ansys-aqwa.

[7]   J. G. Bretl. "A time domain model for wave induced motions coupled to energy extraction." In: *PhD thesis, University of Michigan* (2009).

[8]   C. Chauvigné. "Tenue à la mer d'un flotteur animé de grands mouvements pour les Energies Marines Renouvelables." In: *PhD thesis, Ecole Centrale de Nantes* (2016).

[9]   W. E. Cummins. "The impulse response function and ship motions." In: *Technical report, Department of the Navy* (1962).

[10]   Guillaume Ducrozet. "Water Waves and Sea States Modelling Course note." In: Sept. 2020.

[11]   Pierre Ferrant. "Wave-Structure Interactions class notes." In: 2020.

[12]   G. J. Grigoropoulos and et. al. "Experimental verication of the linear and non-linear versions of a panel code." In: *International Journal of Naval Architecture and Ocean Engineering* 1 (Mar. 2011), pp. 27–36. DOI: 10.3744/JNAOE.2011.3.1.027.

[13]   Y. Huang. "Nonlinear ship motions by a Rankine panel method." In: 1997.

[14]   K. H. Kim and et. al. "Time-domain analysis of nonlinear ship motion responses based on weak-scatterer hypothesis." In: 2009.

[15]   L. D et. al. Landau. In: *Fluid Mechanics (2nd ed.)* 1984.

[16]   L. Letournel. "Développement d'un outil de simulation numérique basé sur l'approche weak-scatterer pour l'étude des systèmes houlomoteurs en grands mouvements." In: *PhD thesis, Ecole Centrale de Nantes* (2015).

[17] Lucas Letournel and et. al. "Comparison of fully non linear and weakly nonlinear potential flow solvers for the study of wave energy converters undergoing large amplitude of motions." In: *ASME 33rd International Conference on Ocean, Offshore and Artic Engineering (OMAE2014)* (June 2014). DOI: 10.1115/OMAE2014-23912.

[18] W. M. Lin and et. al. "Large amplitude motions and wave loads for ship design." In: 1994.

[19] M. S. Longuet-Higgins and Cokelet. "The deformation of steep surface waves on water, I. A numerical method of computation." In: *Royal Society A* (1976), pp. 1–26.

[20] J. S. Pawlowski. " A nonlinear theory of ship motion in waves." In: *Proceedings of the 19th Symposium on Naval Hydrodynamics* (1992).

[21] J. S. Pawlowski. "On the application of the weak-scatterer hypothesis to the prediction of ship motions in heavy seas." In: (1992).

[22] J. S. Pawlowski and D. W. Bass. " A theoretical and numerical model of ship motions in heavy seas." In: *SNAME Transactions* 99 (1992).

[23] J. A. Pinkster. "Low Frequency Second Order Wave Exciting Forces on Floating Structures." In: *PhD thesis, Technical University Delft* (1980).

[24] R. A. Watai. "A time-domain boundary elements method for the seakeeping analysis of offshore systems." In: *PhD thesis, University of Sao Paulo* (2015).

[25] Pierre-Yves Wuillaume. "Numerical simulation of installation operations for offshore wind farms." In: *École centrale de Nantes* (2019). ISSN: 2077-1312. URL: https://www.mdpi.com/2077-1312/8/12/962.

[26] Pierre-Yves Wuillaume. "WS_CN User manual." In: 2019.